Two Current Systems in the Preliminary Phase of Sudden Commencements in the Magnetosphere

Shigeru Fujita (sfujita@ism.ac.jp)
Institute of Statistical Mathematics: Tokei Suri Kenkyujo https://orcid.org/0000-0001-9739-9596
Takashi Tanaka
Kyushu University: Kyushu Daigaku

Research Article

Keywords: Sudden commencement, preliminary impulse, magnetospheric current system, longitudinal propagation speed, computer simulation, generation of the field-aligned current

Posted Date: January 13th, 2022

DOI: https://doi.org/10.21203/rs.3.rs-1199914/v1

Two Current Systems in the Preliminary Phase of Sudden Commencements in the Magnetosphere

Shigeru Fujita[1,2] and Takashi Tanaka[3]

[1] Joint Support-Center for Data Science Research, Research Organization of Information and Systems (ROIS), Tachikawa, Tokyo, Japan 190-8518,

[2] The Institute of Statistical Mathematics, ROIS, Tachikawa, Tokyo, Japan 190-8518, sfujita@ism.ac.jp

[3] International Center for Space Weather Science and Education, Kyushu University, Fukuoka, Japan, 819-0395 tatanaka@serc.kyushu-u.ac.jp

The corresponding author: SF

Abstract

The geomagnetic variations of the preliminary impulse (PI) of the sudden commencement (SC) are known to show a time delay of the peak displacement and longer duration time in the higher latitudes in the pre-noon and post-noon sectors of the polar region. This peculiar behavior of the PI geomagnetic variation is associated with temporal deformation of the ionospheric PI field-aligned current (FAC) distribution into a crescent shape; its lower-latitude edge extends toward the anti-sunward direction, and its higher-latitude edge almost stays on the same longitude near noon. Numerical simulations revealed that the deformation of the FAC distribution is derived from different behaviors of the two PI current systems. The first current system consists of the FAC connected to the PI FAC in the lower latitude side of the ionosphere, the cross-magnetopause current, and the magnetosheath current (type L current system). The cross-magnetopause current is the inertia current generated in the acceleration front of the solar wind due to the sudden compression of the magnetosheath. Thus, the longitudinal speed of the type L current system in the ionosphere is the solar wind speed in the magnetosheath projected into the ionosphere. In contrast, the PI current system connected to the PI FAC at higher latitude (type H current system) consists of the upward/downward FAC in the pre-noon/post-noon sector, respectively, and dawn-to-dusk field-perpendicular current (FPC) along the dayside magnetopause. The dawn-to-dusk FPC moves to the higher latitudes in the outer magnetosphere over time. The FAC of the type H current system is converted from the FPC due to convergence of the return FPC heading toward the sunward direction in the outer magnetosphere; the return FPC is the inertia current driven by the magnetospheric plasma flow associated with compression of the magnetopause behind the front region of the accelerated solar wind.

The acceleration front spreads concentrically from the subsolar point. Consequently, as the return FPC is converted to the FAC of the type H current system, it does not move much in the longitudinal direction over time because the dawn-to-dusk FPC of the type H current system moves to the higher latitudes. Therefore, the high-latitude edge of the PI current distribution in the ionosphere moves only slightly. Finally, we clarified that the FPC-FAC conversion of the type L current system mainly occurs in the region where the Alfvén speed starts to increase toward the Earth. A region with a steep gradient of the Alfvén speed like the plasmapause is not always necessary for conversion from the FPC to the FAC. We also suggest the possible field-aligned structure of the standing Alfvén wave that may occur in the PI phase.

Keywords

Sudden commencement, preliminary impulse, magnetospheric current system, longitudinal propagation speed, computer simulation, generation of the field-aligned current

1 Introduction

The sudden commencement (SC) is an impulse response of the magnetosphere-ionosphere system caused by a sudden change of dynamic pressure of the solar wind [Chapman and Ferraro, 1940]. Therefore, the SC attracts the interest of many scientists as a unique tool for diagnosing the magnetosphere-ionosphere system [Araki, 1994, and references therein]. The characteristic ground magnetic signature of the SC is a simple stepwise change of the north-south component in the middle- and low-latitude regions (referred to as DL after Araki [1994]). In contrast, the ground magnetic variation of the

61 north-south component exhibits a bipolar change in the high-latitude region (DP after
62 Araki [1994]). The first and second variations of the bipolar DP change are called the
63 preliminary impulse (PI) and the main impulse (MI).
64
65 In general, the PI is regarded to be accompanied by upward/downward field-aligned
66 currents (FACs) in the pre-noon/post-noon ionosphere, respectively [Araki, 1994].
67 Tamao [1964] theoretically explained the cause of the PI current system. That is to say,
68 the fast magnetosonic wave generated by sudden compression of the dayside
69 magnetosphere is converted to the Alfvén wave with the upward/downward FAC
70 propagating to the pre-noon/post-noon ionosphere, respectively.
71
72 Global magnetohydrodynamic (MHD) simulations have become a powerful tool for
73 studying the SC [e.g., Fujita et al., 2003a,b]. Fujita et al. [2003a] demonstrated that
74 computer simulation can reproduce realistic ground magnetic variations in the SC
75 period (hereafter Fujita et al. [2003a] is shortened as “Paper 1”). Furthermore, they
76 discussed that the essential mechanisms in the PI current system are fast magnetosonic
77 waves generated by the sudden compression of the dayside magnetosphere, as well as
78 mode conversion from the fast magnetosonic wave to the Alfvén wave due to the spatial
79 gradient of the Alfvén speed, guided by the theory presented by Tamao [1964, 1965]
80 and Araki [1994]. Conversely, in the MI phase, the localized convection vortex cell (the
81 SC transient vortex) in the MI phase plays an essential role in the transient process of
82 the magnetosphere-ionosphere system approaching the new stationary state after
83 compression of the dayside magnetosphere by the solar wind with increased dynamic
84 pressure [Fujita et al., 2003b].

85

86 Paper 1 found a PI current system that schematically resembles the current model by
87 Araki (1994), but they did not further pursue the implications of the simulation results.
88 For example, the longitudinal propagation speed of the PI current system in the
89 magnetosphere will be as fast as that of the fast magnetosonic wave because the FAC is
90 converted from the FPC of the fast magnetosonic wave in the front of the propagating
91 fast magnetosonic wave. However, Engebretson et al. [1999] demonstrated that the
92 longitudinal speed of the PI signal in the ionosphere corresponds to the solar wind
93 speed, not that of the fast magnetosonic wave. In addition, there are issues that Paper 1
94 did not answer; Sastri et al. [2001] indicated that the duration of the ground magnetic
95 variations of the PI in the afternoon (~15 MLT) is longer at higher latitudes. Also, the
96 peak of the variation is delayed at a higher latitude. Takeuchi et al. [2000] also
97 presented the same behavior of the PI geomagnetic variations for the negative SI.
98 Recently, Belakhovsky et al. [2017] also demonstrated a delay in the geomagnetic peak
99 variation of the PI toward the polar region for events in the morning sector (~8.5 MLT).
100 These features, that is, slow longitudinal propagation and peculiar latitudinal change of
101 the PI signal, also seem to appear in the simulation results. For example, the latitudinal
102 change of the PI variation presented in Figure 2 of Paper 1 exhibits the peculiar
103 behavior consistent with the observed one, although they did not mention this behavior.
104 These features are not resolved yet by theoretical and simulation studies. Therefore, we
105 are pursuing explanations of these features in the present paper.
106

107 Furthermore, Paper 1 discussed only qualitatively the conversion from FPC to FAC
108 based on the mode conversion between the fast magnetosonic wave and the Alfvén

wave in the non-uniform distribution of the Alfvén speed in the magnetosphere. Paper 1 concluded that the mode conversion mainly occurs in the region of the steep gradient at Alfvén speeds, and one candidate of the conversion region is the plasmapause. However, they did not study the conversion quantitatively. Because we have the simulation results that satisfy the physical principles of the conversion region, we can investigate quantitatively the conversion from FPC to FAC. This issue is also treated in this paper.

The present paper is structured as follows. Section 2 demonstrates that the ground magnetic variations reproduced by the newly developed global MHD simulation named REProduce Plasma Universe (REPPU) [Tanaka, 2015] can simulate the ground magnetic variation of the SC correctly. Section 3 presents the PI current system in the magnetosphere to reveal the peculiar behaviors of the ground magnetic variations. Section 4 analyses in detail the FPC-FAC conversion in the PI current system. Propagation of the PI signal in the longitudinal direction is also summarized here. The last section summarizes the main results.

2 Preliminary impulse reproduced by the REPPU code

The present simulation study uses the global MHD simulation code REPPU newly developed by Tanaka [2015]. This code solves the MHD equations with the ionospheric boundary condition in the magnetosphere-ionosphere system. The outer boundaries of the magnetosphere are located at 600Re in the dayside and 200Re in the nightside. The inner boundary is set on the sphere with a radius of 3Re. The simulated FAC on the lower boundary is transmitted along the field lines to the ionosphere. The electric field

induced in the ionosphere by the FAC is again transmitted to the magnetosphere. The level 6 version of the REPPU code that we employed for this study has 61,440 triangular surface cells on one sphere and 240 radial layers, so the total number of grid elements is 14,745,600. (The horizontal mesh size is about 0.1Re on the sphere of r=10Re, and the distance between the spheres is about 0.2Re.) Details of the REPPU code are explained in Tanaka [2015]. We imposed a sudden increase in the solar wind plasma density from 10.0 cm^{-3} to 25.0 cm^{-3} at x=25Re from the Earth to drive the SC in the northern interplanetary magnetic field (IMF) condition (IMFBz=+4.3 nT). The other parameters used for the simulation are as follows: IMFBx=0, IMFBy=-4.3 nT, Vx=372 km/s, Vy=Vz=0, and the temperature of the solar wind is 10,000,000 degrees.

It is instructive to show the ground magnetic variations of the SC obtained by the present simulation by REPPU. Paper 1 also calculated the ground magnetic variations from the ionospheric Hall current. Strictly speaking, this method can be used under the condition of a uniform ionosphere and vertical incidence of the FAC into the ionosphere. These two assumptions do not hold in the simulation. To present more correct ground magnetic variations, we calculated the variations from the ionospheric Hall and Pedersen currents, as well as the FAC, based on the Biot-Savart law after Tanaka et al. [2020]. (Tanaka et al. [2020] demonstrated that the ground magnetic variation of the SC is mainly produced by the ionospheric Hall current. Therefore, the present results in Figure 1 and the result by Paper 1 are essentially similar. Note that the present results are more correct than those given in Paper 1.) Let us show the latitudinal dependence of temporal variations of the geomagnetic horizontal components at 15 MLT in the latitude range from 60.8 to 78.5 degrees in Figure 1 based on the simulation

157 results by REPPU. The geomagnetic contribution from the magnetospheric current is
158 not included in Figure 1 because it essentially produces the DL geomagnetic variation.
159 The start time (t=0) is the time when the solar wind shock passes x=25Re. Finally, let us
160 discuss the calculated geomagnetic H variation of this figure. The H component
161 variation at 15 MLT clearly shows that the negative PI variation and the following MI
162 variation in the latitudes below about 70 degrees and similar to the typical variations at
163 about 15 MLT presented by Araki [1994]. Furthermore, we recognize that the duration
164 of the PI geomagnetic variation at 15 MLT becomes longer at higher latitudes and the
165 peak of the H variation becomes delayed (see the variations in the latitudes below 75
166 degrees). Therefore, we can obtain the answers to the unresolved issues about the
167 peculiar behaviors of the PI ground signal by analyzing the present simulation results.
168
169 As noted above, the ground magnetic variation is mainly induced by the ionospheric
170 Hall current. Therefore, we need to investigate the temporal variation of the ionospheric
171 potential distribution. Next, as the potential is controlled by the FAC from the
172 magnetosphere, the temporal variation of the FAC distribution is a key parameter for
173 understanding the behavior of the ground magnetic variations as shown in Figure 1.
174 Following this guideline, we investigate the temporal variation of the FAC distribution
175 and the electric potential distribution. Figure 2 shows these distributions in the northern
176 ionosphere of the latitudes of 60–90 degrees. The FAC distribution and the potential
177 distribution before the SC are depicted in the left panels at t=5.2 min. Next, the typical
178 PI current in the ionosphere (downward/upward FAC in the post-noon/pre-noon sector,
179 respectively) appears at t=5.5 min and 5.9 min, as indicated by black arrows. We notice
180 that the ionospheric PI current distribution depicts a crescent shape with the lower-

latitude edge extending in the anti-sunward direction and the higher-latitude edge almost staying at the same longitude. Corresponding to this crescent shape of the ionospheric PI current, the potential distribution shows a similar shape: the positive/negative potential in the post-noon/pre-noon sector extends in the anti-sunward direction in the lower latitude side. Therefore, this varying ionospheric PI current will invoke the peculiar behavior of the PI geomagnetic variation. That is to say, because the FAC in the lower latitudes advances in the anti-sunward direction faster than the FAC at higher latitudes, the peak time of the PI magnetic disturbance appears earlier than that at higher latitudes. Consequently, to understand the mechanism of the peculiar features of the PI geomagnetic variations, we need to clarify the mechanism in the magnetosphere that causes the latitudinal change of the PI current system.

3 Two current systems in the PI phase

3.1 Current systems obtained from the simulation results

Here, we investigate the magnetospheric current systems driving the ionospheric FAC distribution shown in Figure 2 to clarify the mechanism of the temporal deformation of the crescent-shaped FAC distribution that yields the peculiar behavior of the ground magnetic variations in the PI phase. Because the longitudinal shift of the FAC distribution depends on the latitude, we investigated the magnetosphere-ionosphere current systems from the ionospheric footpoints located at the higher-latitude ionosphere (A_H) and the lower-latitude ionosphere (A_L) at t=5.5 min and B_H (higher latitude), B_C (central latitude), and B_L (lower latitude) at t=5.9 min, as marked in Figure 2. The magnetospheric 3D current systems from these footpoints at t=5.5min. and 5.9 min are shown in Figures 3 and 4, respectively. Note that the respective footpoints

shown in Figures 3 and 4 are the projections from the respective points in the ionosphere to the lower boundary of the simulation (r=3Re) along magnetic field lines. The color of current lines denoted as $J_{\parallel}/|\boldsymbol{J}|$ (blue: antiparallel, white: perpendicular, red: parallel to the magnetic field), where $J_{\parallel}$ and $\boldsymbol{J}$ are the FAC and the current vector, respectively. For convenience, we call the region where a bundle of the current lines is along the main field lines the inner magnetosphere and the other region the outer magnetosphere. For example, the white broken lines in Figure 3 indicate demarcations between the inner magnetosphere and the outer magnetosphere.

First, let us consider the current systems from A_H and A_L at t=5.5 min shown in Figure 3. The current lines from A_H consist of the following three currents; the downward FAC (red) on the post-noon sector in the inner magnetosphere, the upward FAC (blue) on the pre-noon sector in the inner magnetosphere, and the FPC (white), that flow in the dawn-to-dusk direction in the outer magnetosphere. This current system with the footpoints in the higher-latitude ionosphere (A_H) is named the type H current system. The FPC seems to be converted to the FAC gradually in the outer magnetosphere. (The conversion occurs in the region of L≈8.) The other current lines from the footpoint in the lower-latitude ionosphere (A_L) consist of the downward FAC in the post-noon sector of the inner magnetosphere, the FPC across the magnetopause, and the magnetosheath current. This current system is called the type L current system. The cross-magnetopause current enters the magnetosphere and the FPC-FAC conversion occurs at the boundary between the inner and outer magnetospheres apart from the magnetopause. (The conversion occurs in the region of L≈7.) The magnetosheath current tends to flow along the field lines. This tendency attributes to the generation of the FAC due to the flow shear of the

229 solar wind in front of the magnetopause. (The magnetosheath current is discussed again
230 below.) This current system is newly found by the present study. We noticed that the
231 current lines from the anti-sunward edge of A_H go to the magnetosheath (the L current
232 system). This result indicates that A_H is located at the boundary between the regime of
233 the type H current system and that of the type L current system.
234
235 Next, Figure 4 depicts the three current systems from B_H, B_C, and B_L at t=5.9 min. The
236 current lines from B_H belong to the type H current system, and those from B_L are the
237 type L current system. We note that the dawn-to-dusk FPC of the type H current system
238 from B_H at t=5.9 min moves to a latitude higher than that from A_H at t=5.5 min. The
239 cross-magnetopause current and the magnetosheath current of the type L current system
240 seem disturbed compared with that at t=5.5 min. Probably, the solar wind in the
241 magnetosheath begins to become irregular at t=5.9 min. It is noted that the current lines
242 from B_C consist of both the type H current system and the type L current system. This
243 result indicates that the regime of the type H current system advances toward the anti-
244 sunward direction from A_H at t=5.5 min to B_C at t=5.9 min. Therefore, because B_C is
245 located on the sunward side of B_L, the type H current system always appears behind the
246 type L current system heading in the anti-sunward direction.
247
248 To summarize the results of Figures 3 and 4, we can see that the current systems from
249 A_H (t=5.5 min) and B_H (t=5.9 min) belong to the type H current system, whereas those
250 from A_L (t=5.5 min) and B_L (t=5.9 min) belong to the type L current system.
251 Consequently, because A_H and B_H are located in the same longitude, the immovable
252 higher-latitude edge of the crescent-shaped distribution of the PI current system comes

253 from the behavior of the type H current system. At the same time, the extension of the
254 lower-latitude edge is derived from the behavior of the type L current system.
255 Consequently, the PI current distribution becomes a crescent form with the stable
256 higher-latitude edge and the lower-latitude edge moving in the anti-sunward direction
257 due to the coexistence of the two current systems in a different manner of longitudinal
258 spread.
259
260 Because Figure 3 shows only the type L current system with the ionospheric footpoints
261 on the post-noon sector, we show the conjugate type L current systems with the
262 ionospheric footpoints on the pre-noon sector in Figure 5 as well as that from the post-
263 noon sector shown in Figure 3. The 3D equi-contour surface of the pressure roughly
264 corresponds to the dayside magnetopause. The current system in the post-noon sector
265 goes to the magnetosheath in the northern hemisphere, whereas that in the pre-noon
266 sector goes to the magnetosheath in the southern hemisphere. Both currents from both
267 hemispheres flow along the field line in the magnetosheath. Because IMFBy is negative
268 and IMFBz is positive in this simulation as shown in this figure, the current from the
269 post-noon magnetosphere goes to the northern hemisphere. In other words, when
270 IMFBy is positive (and IMFBz is positive), the current system in the post-noon/pre-
271 noon sector goes to the southern/northern magnetosheath, respectively. The
272 magnetosheath current finally connects to the solar wind.
273
274 Note that the current system treated here is a line connecting current vectors at an
275 instant in time; in other words, we are examining snapshots of a constantly changing
276 current line. Thus, although the current line of the type L current system crosses the

277 magnetopause, this does not mean that plasmas in the magnetosheath enter the
278 magnetosphere. When some accelerated plasmas in the magnetosheath deform the
279 magnetopause, adjacent plasmas just inside and outside of the magnetopause move in
280 the same direction. Deformation of the magnetic field associated with this movement
281 will yield the local electric current perpendicular to the magnetopause. However, the
282 plasmas in the magnetosheath do not enter the magnetosphere.
283
284 **3.2 Excitation processes of the two current systems**
285 Now, we discuss how the sudden compression of the dayside magnetosphere excites
286 the type H current system and the type L current system. The important issues are 1)
287 why the type L current system crosses the magnetopause and 2) why the type H current
288 system appears behind the type L current system and the ionospheric footpoint in the
289 higher latitude does not move in the longitudinal direction. In this section, we mainly
290 analyze the current systems at t=5.5 min (Figure 3) because disturbances in the
291 magnetosphere caused by the sudden compression show typical and clear behavior at
292 this time. To tackle these issues, we investigated the spatial patterns of the FPC vectors
293 and the plasma flow vectors in the outer magnetosphere and the magnetosheath. We also
294 analyzed the plasma disturbances in the equatorial plane, although the cross-
295 magnetopause current of the type L current system and the FPC-FAC conversion of the
296 type H current system does occur in the off-equatorial region. This is because both
297 phenomena exist near the equatorial plane and the flow patterns and the FPC patterns in
298 and around the equatorial plane are very similar.
299
300 In the beginning, let us examine the behavior of the FPC in the outer magnetosphere

301 and the magnetosheath at t=5.5 min. Figure 6 shows the FPC vectors in the post-noon
302 sector of the equatorial plane, with $\nabla_\perp \cdot \boldsymbol{J}_\perp$ where $\boldsymbol{J}_\perp$is the FPC vector. The red circle is
303 the projection of the area where the type L current system crosses the magnetopause to
304 the equatorial plane as depicted in Figure 3. Similarly, the area marked by the blue
305 ellipse is the projection of the area where the FPC is converted to the FAC in the type H
306 current system as depicted in Figure 3. We recognize that some current vectors in the
307 red circle direct inward in the magnetopause region. Thus, we need to investigate the
308 driving mechanism of the inward current to understand why the type L current system
309 flows across the magnetopause to understand the first issue. Next, we note that the FPC-
310 FAC conversion for the type H current system appears in the area marked by the blue
311 ellipse where $\nabla_\perp \cdot \boldsymbol{J}_\perp$ is negative. This region is located behind the cross-magnetopause
312 current of the type L current system. Thus, we need to investigate the generation
313 mechanism of negative $\nabla_\perp \cdot \boldsymbol{J}_\perp$ to understand the second issue.
314
315 Now we consider the driving mechanism of the cross-magnetopause current of the
316 type L current system and the generation mechanism of the negative $\nabla_\perp \cdot \boldsymbol{J}_\perp$ of the type
317 H current system. Paper 1 demonstrated that the inertia current ($\boldsymbol{J}_i = \hat{e} \times \left(\rho \frac{D\boldsymbol{v}}{Dt}\right)_\perp / B$) is
318 dominant over the diamagnetic current ($\boldsymbol{J}_d = \hat{e} \times \nabla_\perp p/B$) in the PI phase, where $\mathbf{v}$, p,
319 and $\hat{e}$ denote the flow vector, plasma pressure, and unit vector along the magnetic field
320 ($\boldsymbol{B}/B$), respectively. Consequently, we examined the behavior of the inertia current in
321 the PI phase. (In addition, it is difficult for the diamagnetic current to derive the FPC
322 from the magnetosheath to the magnetosphere because the inward-flowing diamagnetic
323 current in the post-noon sector needs the pressure increase toward the night-side

magnetosheath.) Figure 7 shows the equatorial distribution of the inertia current at t=5.5 min in the post-noon sector. Because in the red circle region, the inertia current has a component that crosses the magnetopause, we understand that the cross-magnetopause current is driven by an inertial force. Next, we recognize that the inertia current in the region between the red circle and the blue ellipse returns toward the noon direction. Furthermore, the inertia current converges in the blue ellipse. Consequently, the convergence of the FPC in the blue ellipse shown in Figure 6 is derived from the behavior of the return inertia current. Therefore, by this return flow, the FPC-FAC conversion region for the type H current system appears behind the region where the type L current system is across the magnetopause.

To understand the behavior of the inertia current, that is, the inward cross-magnetopause FPC and negative $\nabla_{\perp} \cdot \boldsymbol{J}_i$ behind the region of the cross-magnetopause current in Figure 7, we investigated the plasma flow pattern in the post-noon sector of the equatorial plane. Figure 8 shows plasma flow vectors in the outer magnetosphere and the magnetosheath in the post-noon sector of the equatorial plane at t=5.5 min. The color shading indicates the pressure distribution in the equatorial plane. This figure shows that the high-speed magnetosheath flow associated with the sudden compression of the dayside magnetosheath splits to the post-noon sector in the magnetosheath. This high-speed flow in the magnetosheath is caused by squeezing the plasmas in the noon magnetosheath, which is compressed by a sudden increase in the solar wind dynamic pressure. As explained below, plasmas in the front of the high-speed flow are accelerated in the anti-sunward direction along the magnetosheath. Consequently, the inertia force in the anti-sunward direction appears in the front region of the high-speed

348 flow in the red circle, and the inertia current driven by this acceleration generates the
349 cross-magnetopause current from the magnetosheath to the magnetosphere.
350 Furthermore, the flow vectors in Figure 8 explain why the inertia current returning to
351 the sunward direction appears behind the red circle (Figure 7). That is to say, the flow
352 direction gradually deflects from the anti-sunward direction to the Earthward direction
353 in the region between the red circle and the blue ellipse. This flow pattern yields the
354 return flow of the inertia current in the region between the red circle and the blue ellipse
355 shown in Figure 6.
356
357 Let us consider the reason why the high-latitude edge of the type H current system in
358 the ionosphere does not move much in the longitudinal direction from 5.5 min to 5.9
359 min. To explain this feature, we show in Figure 9 the FPC vectors and $\nabla_\perp \cdot \boldsymbol{J}_\perp$ on the
360 sphere of r=8Re at t=5.9 min. The FPC vectors in the region of negative $\nabla_\perp \cdot \boldsymbol{J}_\perp$ head in
361 the sunward direction. This behavior indicates that a return inertia current appears even
362 in the higher latitudes, as in the equatorial region shown in Figure 6. Thus, even at
363 higher latitudes, a negative $\nabla_\perp \cdot \boldsymbol{J}_\perp$ appears in the outer magnetosphere behind the front
364 of the high-speed magnetosheath flow. Furthermore, the nearly concentric distribution
365 of negative $\nabla_\perp \cdot \boldsymbol{J}_\perp$ on the sphere indicates that the deformation of the dayside
366 magnetosheath by the SC spreads concentrically from the subsolar point. Because the
367 dawn-dusk flow of this current at 5.9 min appears at high latitudes as shown in Figure 4,
368 the region where the FPC is converted to FAC shifts rather to the higher latitudes
369 without significant movement toward the anti-sunward direction. Indeed, the conversion
370 region is found in the higher latitude region, as noted with a red circle in this figure.
371 Consequently, the ionospheric footpoint of the type H current system in the higher

372 latitude does not move much in the longitudinal direction. Finally, we can understand
373 the deformation of the FAC distribution in the ionosphere from the high-speed moving
374 type L current system in the lower latitude and the nearly immovable type H current
375 system at higher latitudes. Finally, the fact that the ionospheric footpoint of the type H
376 current system advances from A_H at 5.5 min to B_C at 5.9 min can be explained by the
377 concentric spread of negative $\nabla_\perp \cdot \boldsymbol{J}_\perp$.
378
379 Here, to clarify the acceleration mechanism that drives the cross-magnetopause inertia
380 current, we explain the generation mechanism of the high-speed flow in the red circle
381 shown in Figure 8 from the viewpoint of energy conversion. That is to say, we show
382 how plasmas in the red circle are accelerated. Figure 10 illustrates the equatorial
383 distributions of (a) the work done by the inertia force ($\boldsymbol{v}_\perp \cdot \left(\rho \frac{D\boldsymbol{v}}{Dt}\right)_\perp$), (b) the negative
384 work done by the pressure gradient force ($\boldsymbol{v}_\perp \cdot \nabla_\perp p$), and (c) the work done by the
385 Lorentz force ($\boldsymbol{J}_\perp \cdot \boldsymbol{E}_\perp$). It is evident from this figure that the plasmas are accelerated in
386 the post-noon sector of the magnetosheath ($\boldsymbol{v}_\perp \cdot \left(\rho \frac{D\boldsymbol{v}}{Dt}\right)_\perp > 0$). This region corresponds
387 to the front of the high-speed flow from Figure 8. In addition, because $\boldsymbol{v}_\perp \cdot \nabla_\perp p < 0$ in
388 this region, plasmas are accelerated by the pressure gradient force. When the pressure in
389 the dayside magnetosheath increases suddenly at the onset of the SC, a steep pressure
390 gradient appears in the post-noon sector (and pre-noon sector) of the magnetosheath.
391 Therefore, the compressed dayside magnetosheath squeezes the plasmas in the dayside
392 magnetosheath to the post-noon sector and pre-noon sector of the magnetosheath. Note
393 that $\boldsymbol{J}_\perp \cdot \boldsymbol{E}_\perp$ is positive in the front region of the high-speed flow. In other words, the
394 Lorentz force also accelerates the plasma.

395

396 Finally, we note that $\boldsymbol{J}_{\perp} \cdot \boldsymbol{E}_{\perp}$ is negative in the dayside magnetosheath and dayside
397 magnetopause region. The dynamo of the type H current system is located in the
398 magnetopause region. This dynamo is the same as that for the PI current system
399 reported by Paper 1. In addition, the dynamo in the dayside magnetosheath drives the
400 type L current system.
401
402
403 **4 Discussion**
404 **4.1 Longitudinal propagation of the SC signal in the magnetosphere**
405 Araki (1994) suggested that the front of the SC signal propagates at the speed of the
406 fast magnetosonic wave in the magnetosphere. Moreover, it was already reported that
407 the magnetospheric signal propagates at the speed of the fast magnetosonic wave in the
408 magnetosphere [e.g., Takahashi et al., 2015, 2017]. However, the type L current system
409 propagates in the anti-sunward direction at the speed of the plasma flow in the
410 magnetosheath. This speed is slower than the fast magnetosonic wave speed. Thus, we
411 evaluated the relationship between the speed of the longitudinal propagation of the two
412 current systems introduced in this paper and the magnetosonic speed of the fast
413 magnetosonic wave.
414
415 Figure 11 depicts the temporal propagation of the plasma disturbances ($|dv/dt|$) in the
416 equatorial plane of the magnetosphere-magnetosheath region excited by sudden
417 compression of the dayside magnetosphere. The SC front observed by satellites
418 [Takahashi et al., 2015, 2017] is recognized by the propagating edge of finite $|dv/dt|$ in

this figure. From Figure 11, it is evident that the SC signal front indicated by black thick arrows appears at t=4.0 min in the magnetosphere and propagates toward the nighttime magnetosphere till it arrives at the midnight magnetosphere at t=5.9 min. The propagation speed is about 1000 km/s, which is comparable to the speed of the fast magnetosonic wave (the Alfvén speed) in the magnetosphere. In contrast, the SC signal speed in the magnetosheath (indicated by blue arrows) is almost the solar wind speed (372 km/s). The cross-magnetopause current of the type L current system flows in the SC signal front in the magnetosheath. Consequently, the longitudinal propagation speed of the ionospheric FAC associated with the type L current system is the solar wind speed projected onto the ionosphere. That is to say, the longitudinal propagation speed of the PI signal of the SC caused by the type L current system is slower than that of the SC front determined by the onset of the SC signal in the magnetosphere. The observational fact that the PI signal in the ionosphere propagates at the speed corresponding to the solar wind speed [Engebretson et al., 1999] can be explained by the propagation property of the type L current system. The type H current system follows behind the type L current system.

4.2 Wave modes of the PI current system

As shown in Figures 3 and 4, the FACs in the ionosphere are converted from the FPC in the magnetosphere. The conversion was a key issue of the generation mechanism of the PI geomagnetic variations in terms of coupling of the fast magnetosonic wave and the Alfvén wave [Tamao, 1964]. It is noted that this conversion occurs in the dayside magnetosphere where the plasma β is low. The low β plasma contains the Alfvén wave and the fast magnetosonic wave. Thus, before investigating the FPC-FAC conversion, it

443 is instructive to examine whether the PI current has the nature of the Alfvén-mode
444 current or that of the fast magnetosonic-mode current. In this section, we describe the
445 investigation of the wave modes of the currents both for the type L current system and
446 for the type H current system. In addition, we consider the relationship between the PI
447 current system found by Paper 1 and the type H and type L current systems shown in
448 this paper.
449
450 We evaluated the relative importance of the two MHD waves on the current lines
451 shown in Figure 3. Because the Alfvén wave and the fast magnetosonic wave are
452 characterized by the divergence of the electric field ($\nabla_\perp \cdot \boldsymbol{E}_\perp$) and the field-aligned
453 component of the electric field vortex [$\hat{e} \cdot (\nabla \times \boldsymbol{E}_\perp)$], Figure 12 presents the current
454 lines of the type L current system and the type H current system with the line color of
455 $\epsilon = \frac{\nabla_\perp \cdot \boldsymbol{E}_\perp}{|\nabla_\perp \cdot \boldsymbol{E}_\perp| + |\hat{e} \cdot (\nabla \times \boldsymbol{E}_\perp)|}$ at t=5.5 min. Only the part of the current line in the area with
456 plasma β <0.2 is shown in this figure. When ϵ is close to 0 or ± 1, the current belongs
457 to the fast magnetosonic wave or the Alfvén wave, respectively. From this figure, we
458 recognize that both the type H current system and the type L current system in the inner
459 magnetosphere denoted by (1) have the nature of the Alfvén wave. Next, the dawn-to-
460 dusk current of the type H current system in the outer magnetosphere has the nature of
461 the fast magnetosonic wave. In addition, the cross-magnetopause current of the type L
462 current system has the same nature, too. Both current lines are denoted by (2). Third, we
463 need to discuss the mode of the current connecting the dawn-to-dusk FPC and the FAC
464 of the type H current system along the current lines of (3). We already observed that the
465 dawn-to-dusk FPC of the type H current system seems to be directly converted to the

FAC in Figure 3 because the white current (FPC) curve seems to connect to the red (FAC) one. In contrast, the mode of the current connecting the FPC and the FAC is instead the fast magnetosonic wave from Figure 12 because the color of the current line is white in this figure. This simulation result indicates that the current in the region (3) is a mixture of the Alfvén wave and the fast magnetosonic wave. These patterns are discussed in the next section from the viewpoint of the FPC-FAC conversion.

In the last part of this section, let us discuss the PI current system found by Paper 1. Figure 3 shows that the type H current system from A_H at t=5.5 min, located in the boundary between two regimes, possesses the short FPC between the dawn-to-dusk current and the FAC. This short FPC flows toward the magnetosphere. (The type H current system from B_C at t=5.9 min also consists of the upward/downward FACs and the FPC along the magnetopause, as well as the short FPC that turns toward the Earth from Figure 4.) Figure 12 also indicates that this short current flowing to the magnetosphere has the nature of the fast magnetosonic wave. While the PI current system found by Paper 1 has the FPC between the FAC connecting to the ionosphere and the dawn-to-dusk current along the magnetopause. In addition, Paper 1 discussed that the FPC belongs to the fast magnetosonic wave. Therefore, the type H current system near the transition between the type L current system regime and the type H current system regime is the same as the PI current system found in Paper 1. Thus, the PI current system found by Paper 1 is categorized as the type H current system that appears in the area between the type H current system regime and the type L current system regime.

4.3 Conversion mechanism between the FAC and the FPC

FAC generation in the PI phase has been investigated in the context of conversion from the fast magnetosonic wave to the Alfvén wave [e.g., Tamao, 1964; Fujita et al., 2003a]. However, we note that the Alfvén wave has both the FAC and FPC because the displacement current associated with the Alfvén wave flows perpendicular to the magnetic field. Consequently, the mode conversion theory does not completely explain how the FPC is converted to the FAC in Figure 3. In addition, the previous studies treated the mode conversion only qualitatively. Besides, we have the grid-point values of the FPC and the FAC that satisfy the physical principles of the MHD equations. Therefore, we can discuss rigorously the conversion between the FPC and the FAC. That is to say, we use the conservation of the electric current in the magnetic flux as follows:

$$\nabla_{\parallel}\left(\frac{J_{\parallel}}{B}\right)+\frac{\boldsymbol{\nabla}_{\perp}\cdot\boldsymbol{J}_{\perp}}{B}=0, \tag{1}$$

where $J_{\parallel}$ is the FAC. We also use the wave mode information shown in Figure 12 to interpret the FPC-FAC conversion. Here we investigated the mechanism of the FPC-FAC conversion shown in Figure 3. (We discuss only Figure 3 here because the conversion shown in Figure 4 is essentially the same as that in Figure 3.)

First, because the inertia current is dominant in the PI phase, we examined $\boldsymbol{\nabla}_{\perp}\cdot\boldsymbol{J}_{i}/BJ$ instead of $\boldsymbol{\nabla}_{\perp}\cdot\boldsymbol{J}_{\perp}/BJ$ in the type H current system and the type L current system at t=5.5 min, as shown in Figure 13. (Hereafter, we ignore the type L current system from A_H.) When $\boldsymbol{\nabla}_{\perp}\cdot\boldsymbol{J}_{i}<0$, the FPC is converted to the FAC. This FAC generation is located in the region where the FPC from the cross-magnetopause current becomes the

513 FAC for the type L current system at the boundary between the inner and outer
514 magnetospheres, and in the region where the dawn-to-dusk current turns to the FAC in
515 the post-noon sector in the outer magnetosphere for the type H current system. These
516 regions are denoted by (1). Meanwhile, the FPC generation ($\boldsymbol{\nabla}_\perp \cdot \boldsymbol{J}_i > 0$) appears in the
517 region where the FAC turns to the dawn-to-dusk current in the pre-noon outer
518 magnetosphere for the type H current system. This region is denoted by (2). These
519 results are consistent with the FPC-FAC conversion shown in Figure 3. Finally,
520 $\boldsymbol{\nabla}_\perp \cdot \boldsymbol{J}_i > 0$ is also evident in the lower part of the inner magnetosphere in the post-noon
521 sector for both current systems, and $\boldsymbol{\nabla}_\perp \cdot \boldsymbol{J}_i < 0$ appears in the upper part of the inner
522 magnetosphere in the pre-noon sector in the type H current system. These regions are
523 denoted by (3). ($\boldsymbol{\nabla}_\perp \cdot \boldsymbol{J}_i$ in the region (3) will be discussed in Section 4.3.2.) It is noted
524 here that the FAC is not generated in the high-β and low-β transition region [Tanaka,
525 2007] because the diamagnetic current in the PI phase is not effective in the dayside
526 magnetosphere.
527
528 To investigate the mechanism of $\boldsymbol{\nabla}_\perp \cdot \boldsymbol{J}_i$ presented in Figure 13, we divide $\boldsymbol{\nabla}_\perp \cdot \boldsymbol{J}_i/BJ$
529 into the following five terms:
530 Inertia 1:

$$531 \qquad +\rho\left(\frac{D\boldsymbol{v}}{Dt}\right)_\perp \cdot \frac{2\hat{e} \times \boldsymbol{\nabla}_\perp \mathrm{B}}{B^3 J}, \tag{2}$$

532 Inertia 2:

$$533 \qquad -\rho\left(\frac{D\boldsymbol{v}}{Dt}\right)_\perp \cdot \frac{\hat{e} \times \boldsymbol{\nabla}_\perp \rho}{\rho B^2 J}, \tag{3}$$

534 Inertia 3:

$$-\frac{\rho\hat{e}}{B^2J}\cdot\nabla\times\left(\frac{D\boldsymbol{v}}{Dt}\right)_{\perp}, \quad (4)$$

Inertia 4:

$$+\rho\left(\frac{D\boldsymbol{v}}{Dt}\right)_{\perp}\cdot\frac{\hat{\phi}}{\mathrm{R}_c B^2 J}, \quad (5)$$

Inertia 5:

$$+\rho\left(\frac{D\boldsymbol{v}}{Dt}\right)_{\perp}\cdot\frac{\boldsymbol{\nabla}\times\boldsymbol{B}}{B^3 J}, \quad (6)$$

where R_c is the radius of curvature of the magnetic field line, $\hat{\phi}$ is the unit vector azimuthal to the magnetic field line defined as $\hat{e}\times\hat{n}$, and $\hat{n}$ is the unit vector normal to the magnetic field [$\hat{n}=-(\hat{e}\cdot\boldsymbol{\nabla})\,\hat{e}/\mathrm{R}_c$]. Details of the inertia terms are discussed below.

4.3.1 Inertia 1 and Inertia 2

Inertia 1 and inertia 2 are the FPC-FAC conversion due to the spatial gradient of the magnetic field intensity and the conversion due to the spatial gradient of plasma density, respectively. (Note that inertia 1 corresponds to Eq. 4 of Vasyliunas [1970] by changing the inertia force to the pressure gradient force.) After some algebraic operations, Eqs. (2) and (3) become

$$\rho\left(\frac{D\boldsymbol{v}}{Dt}\right)_{\perp}\cdot\frac{2\hat{e}\times\boldsymbol{\nabla}B}{B^3J}-\rho\left(\frac{D\boldsymbol{v}}{Dt}\right)_{\perp}\cdot\frac{\hat{e}\times\boldsymbol{\nabla}\rho}{\rho B^2 J}=\left(\frac{D\boldsymbol{v}}{Dt}\right)_{\perp}\cdot\frac{\hat{e}\times\boldsymbol{\nabla}V_A^2}{\mu_0 V_A^4}, \quad (7)$$

where V_A is the Alfvén speed. Therefore, it is sufficient to examine the right-hand term of Eq. (7) to investigate the effect of the spatially changing plasmas in the magnetosphere during the FPC-FAC conversion. We call this term inertia V_A (Positive and negative patterns of both inertia 1 and inertia 2 show the same distribution along the current as that of inertia V_A.) Figure 14 shows the type H current system and the type L current system colored according to inertia V_A. When we compare the distribution of the

relative importance of the Alfvén wave in the two MHD waves (ϵ in Figure 12) in the current systems with that of inertia V_A, we recognize that inertia V_A has non-zero values in the region where the fast magnetosonic wave has at least a non-zero contribution (the color of the current line is pale red → yellow → white). Therefore, Figures 12 and 14 confirm that inertia V_A refers to mode conversion from the fast magnetosonic wave to the Alfvén wave due to the spatial gradient of V_A.

Next, we investigated the implication of the inertia V_A change on the type L current system shown in Figure 14. Inertia V_A exhibits negative behavior in the upper part of the inner magnetosphere and adjacent outer magnetosphere. This result indicates that the FPC of the fast magnetosonic wave is converted to the FAC of the Alfvén wave. In other words, the Alfvén wave of the type L current system is recharged by the fast magnetosonic wave due to the spatial gradient of V_A in the upper part of the inner magnetosphere and adjacent outer magnetosphere. We first tried to understand this mode conversion by analyzing the plasma behavior shown in Figure 8. Figure 15 illustrates the distribution of V_A in the equatorial plane and in the 14.4 MLT meridian (the local time of the type L current), as well as the type L current system with the line color of V_A. From Figure 8, $\boldsymbol{v}_\perp$ is directed toward the Earth with a slight tilt to the anti-sunward direction in the region L>7. Thus, the ϕ component of $\boldsymbol{v}_\perp$ is positive. Because $\left(\frac{D\boldsymbol{v}}{Dt}\right)_\perp$ is almost parallel to $\boldsymbol{v}_\perp$, $\left(\frac{D\boldsymbol{v}}{Dt}\right)_\perp$ has a positive ϕ component. Next, the term, $\hat{e} \times \boldsymbol{\nabla} V_A$ in Eq. (7) was estimated as $\hat{e} \times (-\hat{n} \cdot |(\hat{n} \cdot \boldsymbol{\nabla}) V_A|) = -\hat{\phi}|(\hat{n} \cdot \boldsymbol{\nabla}) V_A|$. From Figure 15, V_A in the outer magnetosphere exhibits a smaller but non-zero spatial gradient toward the Earth. Therefore, $|(\hat{n} \cdot \boldsymbol{\nabla}) V_A|$ is positive. Consequently, $\left(\frac{D\boldsymbol{v}}{Dt}\right)_\perp \cdot (\hat{e} \times \boldsymbol{\nabla} V_A)$

580 becomes negative. Thus, we can understand that inertia V_A becomes negative in the
581 outer magnetosphere. (In physical terms, the sudden compression of the dayside
582 magnetosphere induces the fast magnetosonic wave ($\boldsymbol{v}_\perp$ in Figure 8), which is converted
583 to the Alfvén wave due to the spatial gradient of V_A.) As a result, the FPC of the type L
584 current system turns into the FAC in the region where V_A starts to increase toward the
585 inner magnetosphere. Meanwhile, Figure 12 indicates that the Alfvén wave is
586 predominant in the inner magnetosphere and that the fast magnetosonic wave does not
587 arrive there. Therefore, inertia V_A becomes almost zero in the inner magnetosphere
588 because there is no fast magnetosonic wave, although the spatial gradient of V_A is
589 enhanced in the inner magnetosphere. In other words, this area is not the region where
590 the spatial gradient of V_A is steep, for example, the plasmapause region, as suggested by
591 Paper 1. This mechanism determines the lower latitude boundary of the FAC of the PI
592 in the ionosphere.
593
594 The behavior of inertia V_A on the type H current system is rather complicated compared
595 with that of the type L current system. It shows roughly two negative regions and one
596 positive region in the post-noon magnetosphere. That is, the FAC is recharged from the
597 fast magnetosonic wave in the near-equatorial region of the outer magnetosphere, it then
598 charges the fast magnetosonic wave in the neighboring region between the inner and
599 outer magnetospheres, and it again recharges the fast magnetosonic wave in the upper
600 edge part of the inner magnetosphere. This structure is related to the profile of inertia 3
601 in the type H current system. Thus, this feature of inertia V_A in the type H current
602 system is discussed below.
603

4.3.2 Inertia 3

Inertia 3, shown in Figure 16, is related to the Alfvén wave because $\hat{e} \cdot \boldsymbol{\nabla} \times \left(\frac{D\boldsymbol{v}}{Dt}\right)_{\perp}$ is roughly proportional to $\boldsymbol{\nabla}_{\perp} \cdot \boldsymbol{E}_{\perp}$. Therefore, this term represents the conversion between the displacement current (FPC) and the FAC within the Alfvén wave. To show the behavior of inertia 3 in the lower boundary, the inset in the left-bottom corner shows an enlarged part of the footpoints of both current systems. The color scale of inertia 3 for the inlet is given in increments of ± 0.05.

First, we describe the characteristic features of inertia 3 in the type L current system. It is essentially positive from the lower boundary to the outer magnetosphere in the post-noon sector. This feature indicates that the Alfvén wave is recharged by the fast magnetosonic wave due to the spatial gradient of V_A in the upper part of the inner magnetosphere and the outer magnetosphere (Figure 14). On the way to the ionosphere, the displacement current of the Alfvén wave diverges from the field line. It is noted that inertia 3 has smaller values but is still positive in the lower boundary region, as seen in the inset of Figure 16. The positive inertia 3 near the lower boundary can be understood as demonstrating that the electric current in the ionosphere has positive divergence because the PI current in this region flows into the ionosphere. The smaller inertia 3 near the lower boundary implies that the PI electric field induced in the ionosphere may be suppressed by the conducting ionosphere.

Second, inertia 3 in the type H current system in the post-noon sector is positive in the lower half part of the inner magnetosphere, and the sign reverses in the upper half. It is

627 noted that inertia V_A in the inner magnetosphere in Figure 14 is negative in the region
628 where inertia 3 is zero. At the same time, $\boldsymbol{\nabla}_\perp \cdot \boldsymbol{J}_i$ is also negative (Figure 13) in the
629 upper part. These results allow us to conclude that convergence of the inertia current
630 (Figure 6) yields an increase in the FAC of the Alfvén wave (negative inertia 3 in
631 Figure 16) and an increase in the FPC of the fast magnetosonic wave (positive inertia V_A
632 in Figure 14). It is noted that the inertia 3 of the Alfvén wave exhibits a field-aligned
633 structure with a node in the inner magnetosphere. In the outer magnetosphere, the
634 Alfvén wave and the fast magnetosonic wave are mixed in the current lines between the
635 dawn-to-dusk current and the FAC of the type H current system. Therefore, inertia 3
636 and inertia V_A have different signs alternately.
637
638 Finally, we discuss whether the behavior of inertia 3 indicates excitation of a standing
639 Alfvén wave. First, the type L current system has smaller inertia 3 in the lower
640 boundary (the ionosphere) and is positive on the current lines. The plasma disturbances
641 in the dayside magnetosphere are symmetric with respect to the equatorial plane, and
642 inertia 3 is positive in the southern hemisphere. Therefore, the global field-aligned
643 profile of inertia 3 exhibits a wave of the field line with nodes in the northern and
644 southern ionospheres and an antinode at the equator. Consequently, the fundamental
645 standing Alfvén wave may be generated in the lower latitude part of the PI current
646 system. However, the wave structure of the field line of the FAC part of the type H
647 current system has positive inertia 3 in the lower part of the inner magnetosphere in
648 both hemispheres and a negative one in the equatorial region. Thus, nodes will appear in
649 between the lower boundary (the ionosphere) and the equator. Therefore, the Alfvén
650 wave with the third harmonic structure is possibly excited in the higher-latitude part of

651 the PI current system. The global MHD simulation cannot reproduce the standing
652 Alfvén wave because of its numerical diffusion. Thus, the simulation does not
653 reproduce the standing waves noted above. To confirm this possible standing wave is a
654 future issue.
655
656 **4.3.3 Inertia 4**
657 Inertia 4 represents the FPC-FAC conversion due to curvature of the magnetic field
658 line. When the magnetic field is almost a dipole field, we obtain
659 $$\frac{\hat{e}\times\boldsymbol{\nabla}B}{B^3}\simeq\frac{\boldsymbol{\nabla}\times\hat{e}}{B^2}=\frac{\hat{\phi}(\hat{n}\cdot\boldsymbol{\nabla})B}{B^3}\simeq-\frac{\hat{\phi}}{R_cB^2}. \quad (8)$$
660 Therefore, the curvature effect (inertia 4) is half the size of inertia 1, and the sign is
661 reversed. As a result, this term does not play an important role in the conversion
662 between the FPC and FAC.
663
664 **4.3.4 Inertia 5**
665 Inertia 5 is derived by modification of the magnetic field direction caused by the
666 current. Eventually, this term can be deformed like
667 $$\rho\left(\frac{D\boldsymbol{v}}{Dt}\right)_\perp\cdot\frac{\boldsymbol{\nabla}\times\boldsymbol{B}}{B^3J}=\rho\left(\frac{D\boldsymbol{v}}{Dt}\right)_\perp\cdot\frac{\boldsymbol{J}_\perp}{\mu_0B^3J}=\rho\left(\frac{D\boldsymbol{v}}{Dt}\right)_\perp\cdot\frac{\boldsymbol{J}_d}{\mu_0B^3J}, \quad (9)$$
668 where μ_0 is the magnetic permeability of a vacuum. This term is not effective in the
669 magnetosphere compared with other terms because $\boldsymbol{J}_d$is not significant in the dayside
670 magnetosphere.
671
672 **4.4 Ionospheric latitudes of the PI current system**
673 To conclude our discussion, we will focus on the ionospheric latitude of the PI current

system. This latitude corresponds to the magnetic field line where the FPC is converted to the FAC. The ionospheric latitude of the PI current in the higher latitudes (the type H current system) and is related to the area where the return inertia current exhibits convergence near the post-noon magnetopause as shown in Figure 6. (The current shows divergence near the pre-noon magnetopause although this is not shown in this figure.) This is located at L≈8. While the PI current in the lower latitudes (the type L current system) exhibits the conversion in the area considerably distant from the magnetopause. From Figure 15, the FPC from the cross-magnetopause current turns to the FAC in the region where V_A begins to increase toward the Earth. This is located at L≈7. It is noted that the turning position does not exist in the region with a steep V_A gradient, although the FPC-FAC conversion occurs due to the spatial gradient of V_A.

5 Summary and conclusion

We performed simulations of the PI current systems in the magnetosphere-ionosphere system and found that there are two different current systems in the PI phase in the higher-latitude region and the lower-latitude region of the ionospheric FAC region of the PI. The main results of this paper are summarized as follows:

1. The PI current system with the FAC in the lower-latitude ionosphere (type L current system) consists of the FAC in the inner magnetosphere and the ionosphere, the cross-magnetopause current, and the magnetosheath current. The cross-magnetopause current is the inertia current invoked by the inertia force to the anti-sunward direction in the front region of the high-speed flow invoked by compression of the dayside magnetosheath. The longitudinal propagation speed of

698 this current system is the solar wind speed in the magnetosheath in the anti-
699 sunward direction projected into the ionosphere. But it is considerably slower than
700 the fast magnetosonic wave in the magnetosphere.
701 2. The PI current system with the FAC in the higher-latitude ionosphere (type H
702 current system) consists of upward/downward FACs in the pre-noon/post-noon
703 sections, respectively, and dawn-to-dusk along the magnetopause in the outer
704 magnetosphere. This current system appears behind the type L current system.
705 The PI current system found by Fujita e al. [2003a] is categorized as the type H
706 current system that appears in the area between the type H current system regime
707 and the type L current system regime.
708 3. The type L current system in the ionosphere propagates in the anti-sunward
709 direction at the solar wind speed in the magnetosheath projected into the
710 ionosphere. In contrast, the type H current system in the ionosphere appears
711 behind the type L current system, and this current system in the sunward edge in
712 the ionosphere almost stays in the same longitude. Therefore, the PI current
713 distribution of the ionosphere forms a crescent shape in which the low-latitude
714 edges extend in the anti-sunward direction and the high-latitude edges are almost
715 stationary. Consequently, the duration of the PI ground magnetic signal becomes
716 longer at higher latitudes, and the peak of the PI geomagnetic variations is delayed
717 at higher latitudes.
718 4. The spatial gradient of plasmas induces conversion from FPC to FAC of the type
719 L current system due to the mode conversion from the fast magnetosonic wave to
720 the Alfvén wave. This conversion occurs in the outer magnetosphere, where the
721 compression of the dayside magnetosphere drives the inward plasma flow that

belongs to the fast magnetosonic wave. Consequently, the FPC turns into the FAC in the region where the Alfvén speed begins to increase toward the inner magnetosphere. This region does not correspond to the region with a steep spatial gradient of the Alfvén speed, like the plasmapause. This mechanism determines the low-latitude limit of the FAC of the PI in the ionosphere.

5. The FPC to FAC conversion for the type H current system occurs in the outer magnetosphere near the magnetopause. The return inertia current from the region where the type L current system crosses the magnetopause invokes negative/positive divergence in the post-noon/pre-noon sector, respectively. Thus, the type H current system always appears behind the type L current system.
6. The conversion between the displacement current (FPC) and the FAC of the Alfvén wave is dominant in the near-Earth inner magnetosphere. The divergence of the displacement current is positive in the post-noon inner magnetosphere for both the type L and type H current systems because downward FAC in the ionosphere invokes a positive divergence of the current in the ionosphere. The positive divergence of the displacement current extends along the current line of the type L current system to the outer magnetosphere. In contrast, the type H current system has a negative divergence in the outer magnetosphere because the inertia current in the post-noon sector of the outer magnetosphere exhibits convergence.
7. The fundamental standing Alfven wave in the lower latitude side of the PI signal and the third harmonic standing Alfven wave in its higher latitude side are possibly excited associated with the SC.

Declarations

Ethics approval and consent to participate

Not applicable.

Consent for publication

Not applicable.

List of abbreviations

DL: SC-related geomagnetic disturbance in the low latitudes

DP: SC-related geomagnetic disturbance in the polar region

FAC: field-aligned current (electric current parallel to the magnetic field line)

FPC: field-perpendicular current (electric current perpendicular to the magnetic field line)

IMF: interplanetary magnetic field

MHD: magnetohydrodynamic

MI: main impulse of the SC

MLT: Magnetic Local Time

PI: preliminary impulse of the SC

SC: sudden commencement

REPPU: REProduce Plasma Universe (magnetosphere-ionosphere coupling global MHD simulation code)

ε: $\frac{\nabla_\perp \cdot \boldsymbol{E}_\perp}{|\nabla_\perp \cdot \boldsymbol{E}_\perp| + |\hat{e} \cdot (\nabla \times \boldsymbol{E}_\perp)|}$

766 **Availability of data and materials**

767 The simulation results used for this paper are available along with IDL
768 programs for reading these data at
769 http://polaris.nipr.ac.jp/~sfujita/exchange/EPS_SC/.

770 **Competing interests**

771 No competing interests

772 **Funding**

773 Japan Society for the Promotion of Science (KAKENHI grant number
774 20K03894).
775 Research Organization of Information and Systems, “Infrastructure
776 development for the global reanalysis data of the magnetosphere-
777 ionosphere system,” supported by a “Challenging Exploratory Research
778 Projects for the Future" grant.

779 **Authors’ contributions**

780 SF conducted the numerical simulation and analyzed the simulation
781 results. SF and TT wrote the paper.

782 **Acknowledgments**

783 This work was stimulated by a discussion with Araki. The simulation
784 was performed with the computers installed at the Center for Engineering
785 and Technical support of the Institute of Mathematical Statistics and the
786 Polar Science Computer System at National Institute of Polar Research.

787

788 **References**

789 Araki, T. (1994) A physical model of the geomagnetic sudden commencement. In: M. J.
790 Engebretson, K. Takahashi, and M. Scholer (ed), Solar Wind Sources of
791 Magnetospheric Ultra-Low-Frequency Waves, American Geophysical Union,
792 Washington, D.C., 183-200.
793
794 Belakhovsky, V. B., V. A. Pilipenko, Ya. A. Sakharov, D. L. Lorentzen and S. N.
795 Samsonov (2017), Geomagnetic and ionospheric response to the interplanetary shock on
796 January 24, 2012, Earth, Planets and Space 69:105, DOI 10.1186/s40623-017-0696-1.
797
798 Chapman, S., and Ferraro, V. C. A. (1940), The theory of the first phase of a
799 geomagnetic storm, Terr. Magn. Atmos. Electr., 45(3), 245-268,
800 doi:10.1029/TE045i003p00245.
801
802 Engebretson, M. J., D. L. Murr, W. J. Hughes, H. Lühr, T. Moretto, J. L. Posch, A. T.
803 Weatherwax, T. J. Rosenberg, C. G. Maclennan, L. J. Lanzerotti, F. Marcucci, S.
804 Dennis, G. Burns, J. Bitterly, and M. Bitterly (1999), A multipoint determination of the
805 propagation velocity of a sudden commencement across the polar ionosphere, J.
806 Geophys. Res., 104(A10), 22433-22451, doi:10.1029/1999JA900237.
807
808 Fujita, S., T. Tanaka, T. Kikuchi, K. Fujimoto, K. Hosokawa, and M. Itonaga (2003a),
809 A numerical simulation of the geomagnetic sudden commencement: 1. Generation of
810 the field-aligned current associated with the preliminary impulse, J. Geophys. Res.,
811 108(A12), 1416, doi:10.1029/2002JA009407.

812

813 Fujita, S., T. Tanaka, T. Kikuchi, K. Fujimoto, and M. Itonaga (2003b), A numerical
814 simulation of the geomagnetic sudden commencement: 2. Plasma processes in the main
815 impulse, J. Geophys. Res., 108(A12), 1417, doi:10.1029/2002JA009763.
816
817 Sastri, J. H., Takeuchi, T., Araki, T., Yumoto, K., Tsunomura, S., Tachihara, H., Luehr,
818 H., and Watermann, J. (2001), Preliminary impulse of the geomagnetic storm sudden
819 commencement of November 18, 1993, J. Geophys. Res., 106(A3), 3905-3918,
820 doi:10.1029/2000JA000226.
821
822 Takahashi, N., Y. Kasaba, A. Shinbori, Y. Nishimura, T. Kikuchi, Y. Ebihara, and T.
823 Nagatsuma (2015), Response of ionospheric electric fields at mid-low latitudes during
824 sudden commencements. J. Geophys. Res. Space Physics, 120, 4849-4862. doi:
825 10.1002/2015JA021309.
826
827 Takahashi, N., Y. Kasaba, Y. Nishimura, A. Shinbori, T. Kikuchi, T. Hori, Y. Ebihara,
828 and N. Nishitani (2017), Propagation and evolution of electric fields associated with
829 solar wind pressure pulses based on spacecraft and ground-based observations, J.
830 Geophys. Res. Space Physics, 122, 8446-8461, doi:10.1002/2017JA023990.
831
832 Takeuchi, T., T. Araki, H. Luehr, O. Rasmussenn, J. Watermann, D. K. Milling, I. R.
833 Mann, K. Yumoto, K. Shiokawa, and T. Nagai, Geomagnetic negative sudden impulse
834 due to a magnetic cloud observed on May 13, 1995. J. Geophys. Res., 105, 18835-
835 18846, 2000.

836

837 Tamao, T., A hydromagnetic interpretation of geomagnetic SSC*, Rep. Ionos. Space
838 Res. Japan, 18, 16-31, 1964.
839
840 Tamao, T., Transmission and coupling resonance of hydromagnetic disturbances in the
841 non-uniform Earth's magnetosphere, Sci. Rep. Tohoku Univ., Series 5, Geophysics, 17,
842 43-72, 1965.
843
844 Tanaka, T. (2007), Magnetosphere-Ionosphere Convection as a Compound System,
845 Space Sci Rev, 133, 1-72, DOI 10.1007/s11214-007-9168-4.
846
847 Tanaka, T. (2015), Substorm auroral dynamics reproduced by the advanced global M-I
848 coupling simulation, In Auroral dynamics and space weather, Geophys. Monogr. Ser.,
849 vol. 215, edited by Y. Zhang and L. J. Paxton, p. 177, doi: 10.1002/9781118978719,
850 AGU, Washington D. C.
851
852 Tanaka, T., Y. Ebihara, M. Watanabe, M. Den, S. Fujita, T. Kikuchi, K. K. Hashimoto,
853 and R. Kataoka (2020), Reproduction of ground magnetic variations during the SC and
854 the substorm form the global simulation and Biot-Savart's law, Journal of Geophysical
855 Research: Space Physics, 125, e2019JA027172. https://doi.org/10.1029/2019JA027172
856
857 Vasyliunas, V. M. (1970), Mathematical Models of Magnetospheric Convection and its
858 Coupling to the Ionosphere, Particles and Fields in the Magnetosphere, 60-71, Ed. by

McCormac, B.M. Springer Netherlands. http://dx.doi.org/10.1007/978-94-010-3284-1_6

862 **Figure legends**

863 Figure 1: Latitudinal dependences of the temporal variations of the H- and D-
864 component ground magnetic fields associated with the SC in the latitudes from 60.8 to
865 78.5 degrees in the northern hemisphere at 15 MLT. The vertical arrow in the right axis
866 in each panel indicates the magnetic variation of 50 nT. The start time (t=0) is the time
867 when the solar wind shock passes x=25Re.

868

869 Figure 2: (top row) Temporal evolution of the FAC distribution in the northern
870 hemisphere at latitudes above 60 degrees from t=5.2 min to 5.9 min. The black arrows
871 at t=5.5 min and 5.9 min indicate the FACs of the PI. The red thick lines labeled A_H and
872 A_L in the 5.5-min panel and B_H, B_c, and B_L in the 5.9-min panel indicate the footpoints
873 of the current systems shown in Figures 3 and 4. The latitude and MLT of these
874 footpoints are as follows: A_H=(75.5 deg, 12.6–13.1 MLT); A_L=(69.1 deg, 14.0–14.8
875 MLT); B_H=(73.6 deg, 12.6–13.1 MLT); B_C=(71.3 deg, 13.8–15.0 MLT); B_L=(65.9
876 deg, 16.2–16.8 MLT). (bottom row) Temporal evolution of the electric potential
877 distribution for the same region and time intervals.

878

879 Figure 3: Snapshots of the electric current systems at t=5.5 min as seen from the post-
880 noon point in the northern hemisphere. The color of the electric current lines denotes
881 $J_{\parallel}/|\boldsymbol{J}|$ (blue: antiparallel, white: perpendicular, red: parallel to the magnetic field). The
882 red and blue shadings in the lower boundary (the sphere of $r = 3\mathrm{R_e}$) indicate
883 downward and upward FACs, respectively. A_H and A_L indicate the projection of both
884 areas in the ionosphere (Figure 2) to the lower boundary. The white arrows represent the
885 directions of the currents. The white dotted lines indicate the demarcation between the

886 inner magnetosphere and the outer magnetosphere. The pressure in the equatorial plane
887 and that in the noon-midnight meridian are shown with color contour lines. The type H
888 current system from A_H consists of two FACs on the pre-noon sector and the post-noon
889 sector and the FPC connecting these two FACs. The type L current system from A_L is
890 made up of the downward FAC and the electric current in the magnetosheath via the
891 FPC across the magnetopause. Some current lines from A_L belong to the type L current
892 system.
893
894 Figure 4: Snapshots of the electric current systems at t=5.9 min in the same format used
895 in Figure 3. B_H, B_C, and B_L indicate the projection of the three areas in the ionosphere
896 (Figure 2) to the lower boundary. The currents from B_H and B_L are, respectively, the
897 type H current system and the type L current system. The currents from B_C belong to the
898 type H current system or the type L current system. The type H current system advances
899 the region of B_C from t=5.5 min to t=5.9 min. Note that the type L current system goes
900 farther in the longitudinal direction.
901
902 Figure 5: Overall picture of the type L current system connected to the ionosphere in the
903 northern hemisphere, as seen from the Sun at t=5.5 min. This figure shows the type L
904 current system from the post-noon ionosphere (the same as that in Figure 3) and that
905 from the pre-noon ionosphere. The type L current from the pre-noon ionosphere goes to
906 the magnetosheath in the southern hemisphere. The 3D equi-contour of the pressure
907 seen from the Sun is shown with volume rendering. The equi-contour roughly indicates
908 the magnetopause. The black arrow in the right indicates IMF direction.
909

910 Figure 6: FPC vectors in the post-noon sector of the equatorial plane at 5.5 min. $\nabla_\perp \cdot \boldsymbol{J}_\perp$
911 values in the equatorial plane are shown with color shading. The red circle indicates the
912 equatorial projection of the region where the cross-magnetopause current exists. The
913 type L current flows across the magnetopause in this region. In contrast, the blue ellipse
914 indicates the equatorial projection of the region where the type H current system
915 converts from the FPC to the FAC. It is evident that the current exhibits negative
916 divergence ($\nabla \cdot \boldsymbol{J}_\perp < 0$) in the blue ellipse.
917
918 Figure 7: Vectors of the inertia current ($\boldsymbol{J}_i$) in the post-noon sector of the equatorial
919 plane at 5.5 min. The pressure distribution in the equatorial plane is shown with color
920 shading. See the Figure 6 caption for descriptions of the red circle and blue ellipse.
921
922 Figure 8: Vectors of the plasma flow perpendicular to the magnetic field in the post-
923 noon sector of the equatorial plane at 5.5 min. The pressure distribution in the equatorial
924 plane is shown with color shading. See the Figure 6 caption for the description of the
925 red circle.
926
927 Figure 9: FPC vectors in the post-noon sector on the sphere of r=8Re in the northern
928 hemisphere at 5.9 min. $\nabla_\perp \cdot \boldsymbol{J}_\perp$ on this sphere is shown with color shading. The red circle
929 indicates the region through which the type L current system from B_H passes (Figure 4).
930
931 Figure 10: Values of (a) $\boldsymbol{v}_\perp \cdot \rho \left(\frac{D\boldsymbol{v}}{Dt}\right)_\perp$, (b) $v_\perp \cdot \nabla_\perp p$, and (c) $\boldsymbol{J}_\perp \cdot \boldsymbol{E}_\perp$ in the post-noon
932 sector of the equatorial plane at t=5.5 min. The line contours of each panel indicate

933 equi-contour lines of the pressure. See the Figure 6 caption for the description of the
934 red circle.
935
936 Figure 11: Temporal spread of the magnetospheric SC signal front, indicated as the edge
937 of the positive region of $|\frac{dv}{dt}|$. The black and blue arrows in the panels of t=4.0 min to
938 t=6.2 min indicate the SC front in the magnetosphere and the magnetosheath,
939 respectively. It is evident that the SC front arrives at the nightside magnetosphere at 6.2
940 min, when the PI current system in the ionosphere does not reach the nightside. The line
941 contours show the pressure in the equatorial plane. Irregular patterns of $|\frac{dv}{dt}|$ in the
942 nightside magnetosphere are fluctuations. We do not discuss the fluctuations in this
943 paper because they do not play any roles in the propagation of the SC signal.
944
945 Figure 12: The type H and L current systems illustrated in the same manner used in Figure
946 3 at t=5.5 min according to the value of ϵ. The current lines are shown only in the area of
947 β<0.2. The Alfven-mode current and the fast magnetosonic-mode current are dominant
948 along the current lines denoted by (1) and (2), respectively. The mixture of the two modes
949 appears along the current lines denoted by (3).
950
951 Figure 13: Type H and L current systems at t=5.5 min colored according to $\frac{\nabla_\perp \cdot \mathbf{J}_i}{JB}$ values
952 in the same manner as in Figure 3. The current lines are shown only in the area of
953 β<0.2. The type L current from A_H is not shown in this figure. There are three
954 characteristic regions of the FPC-FAC conversion. The negative and positive $\frac{\nabla_\perp \cdot \mathbf{J}_i}{JB}$ in
955 regions (1) and (2), respectively, appears in the boundary between the outer and inner

956 magnetosphere. The region (3) is located in the lower magnetosphere.

957

958 Figure 14: Type H and L current systems at t=5.5 min colored according to inertia V_A in
959 the same manner as in Figure 3. The current lines are shown only in the area of β<0.2.
960 The contour line colors change in increments of ± 0.1. The type L current from A_H is
961 not shown in this figure.

962

963 Figure 15: Distributions of V_A in the 14.4 MLT meridian plane and the equatorial plane.
964 The type L current system that flows in the 14.4 MLT plane is also shown. The white
965 dotted arrow indicates the L value of the field line where FPC is converted to FAC
966 (L≈7). The color of the current lines denotes V_A.

967

968 Figure 16: Type H and L current systems at t=5.5 min colored according to inertia 3
969 values in the same manner as in Figure 3. The current lines are shown only in the area
970 of β<0.2. The contour line colors change in increments of ± 0.2. The type L current
971 from A_H is not shown in this figure. The inset in the left-bottom corner shows an
972 enlarged part of the footpoints of both current systems. The color scale of inertia 3 for
973 the inset is in increments of ± 0.05.

Figures

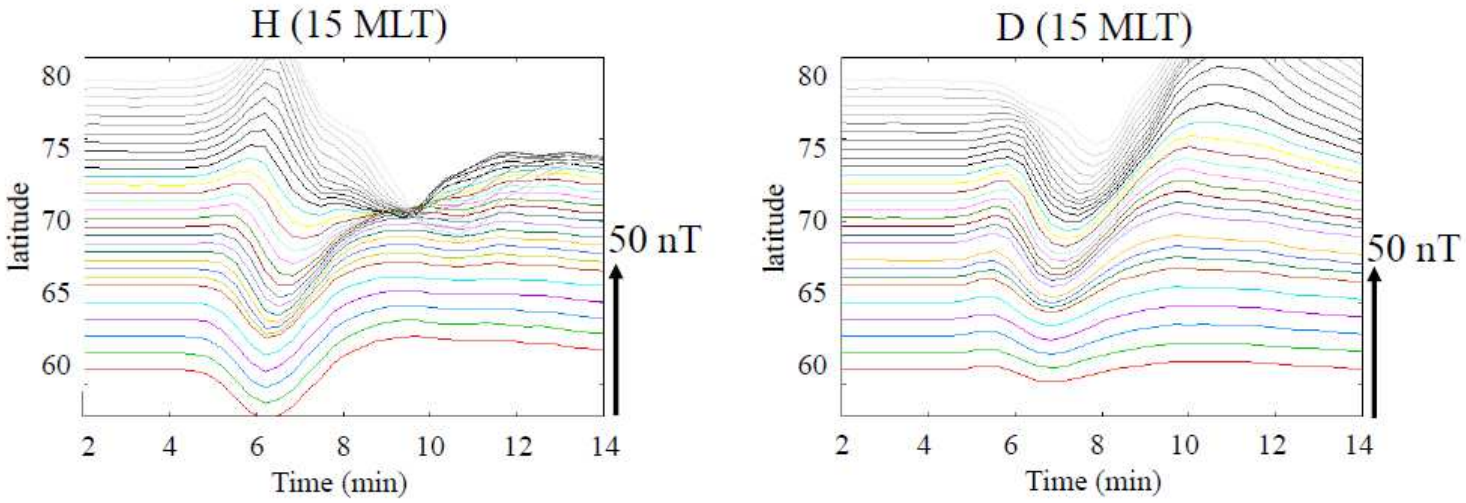

Figure 1

Latitudinal dependences of the temporal variations of the H- and D-component ground magnetic fields associated with the SC in the latitudes from 60.8 to 78.5 degrees in the northern hemisphere at 15 MLT. The vertical arrow in the right axis in each panel indicates the magnetic variation of 50 nT. The start time (t=0) is the time when the solar wind shock passes x=25Re.

Figure 2

(top row) Temporal evolution of the FAC distribution in the northern hemisphere at latitudes above 60 degrees from t=5.2 min to 5.9 min. The black arrows at t=5.5 min and 5.9 min indicate the FACs of the PI. The red thick lines labeled A_H and A_L in the 5.5-min panel and B_H, B_c, and B_L in the 5.9-min panel indicate the footpoints of the current systems shown in Figures 3 and 4. The latitude and MLT of these footpoints are as follows: A_H=(75.5 deg, 12.6–13.1 MLT); A_L=(69.1 deg, 14.0–14.8 MLT); B_H=(73.6 deg, 12.6–13.1 MLT); B_C=(71.3 deg, 13.8–15.0 MLT); B_L=(65.9 deg, 16.2–16.8 MLT). (bottom row) Temporal evolution of the electric potential distribution for the same region and time intervals.

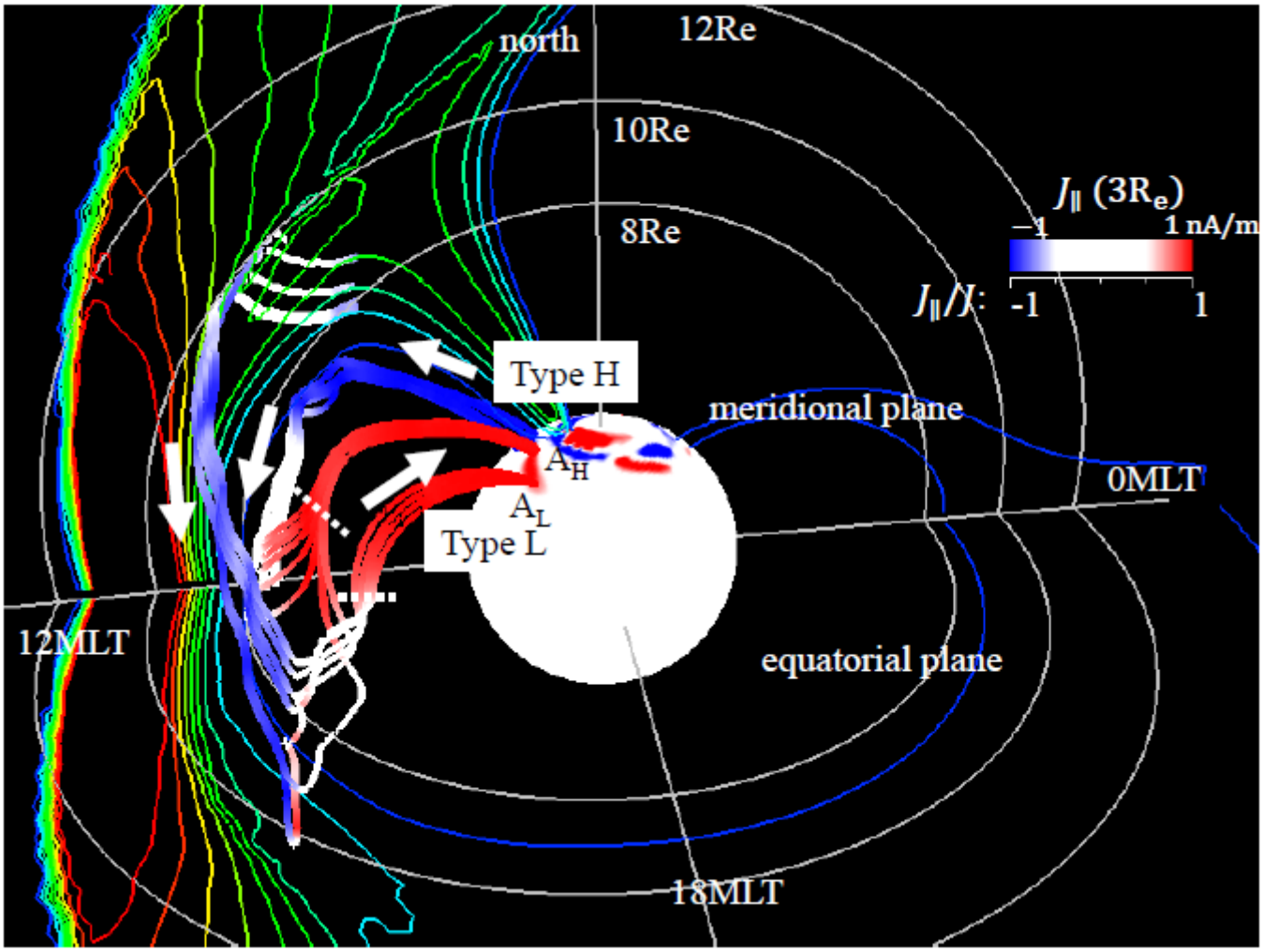

Figure 3

Snapshots of the electric current systems at t=5.5 min as seen from the post-noon point in the northern hemisphere. The color of the electric current lines denotes $J_{\parallel}/|J|$ (blue: antiparallel, white: perpendicular, red: parallel to the magnetic field). The red and blue shadings in the lower boundary (the sphere of $r=3R_e$) indicate downward and upward FACs, respectively. A_H and A_L indicate the projection of both areas in the ionosphere (Figure 2) to the lower boundary. The white arrows represent the directions of the currents. The white dotted lines indicate the demarcation between the inner magnetosphere and the outer magnetosphere. The pressure in the equatorial plane and that in the noon-midnight meridian are shown with color contour lines. The type H current system from AH consists of two FACs on the pre-noon sector and the post-noon sector and the FPC connecting these two FACs. The type L current system from AL is made up of the downward FAC and the electric current in the magnetosheath via the FPC across the magnetopause. Some current lines from AL belong to the type L current system.

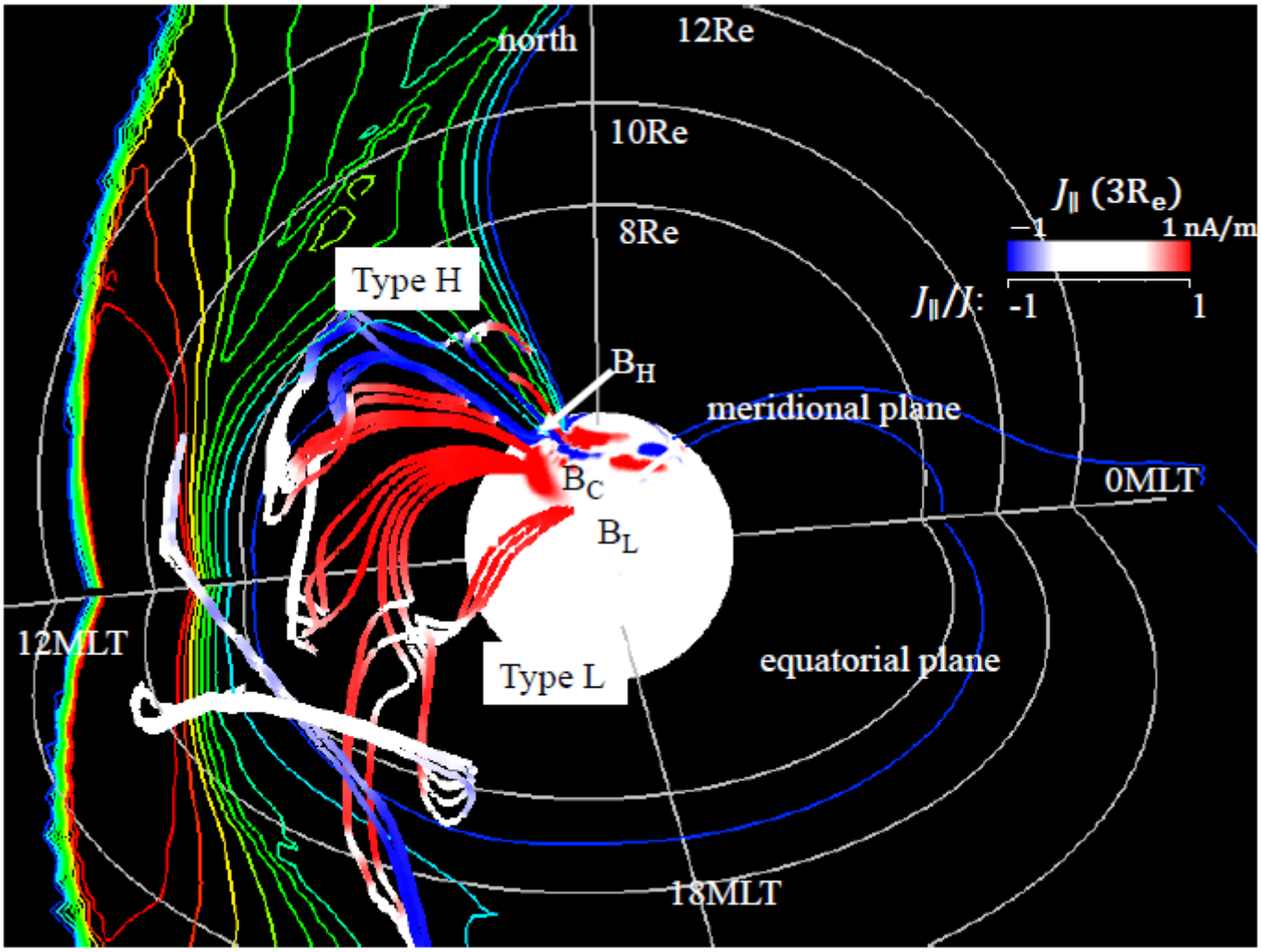

Figure 4

Snapshots of the electric current systems at t=5.9 min in the same format used in Figure 3. B_H, B_C, and B_L indicate the projection of the three areas in the ionosphere (Figure 2) to the lower boundary. The currents from B_H and B_L are, respectively, the type H current system and the type L current system. The currents from B_C belong to the type H current system or the type L current system. The type H current system advances the region of B_C from t=5.5 min to t=5.9 min. Note that the type L current system goes farther in the longitudinal direction.

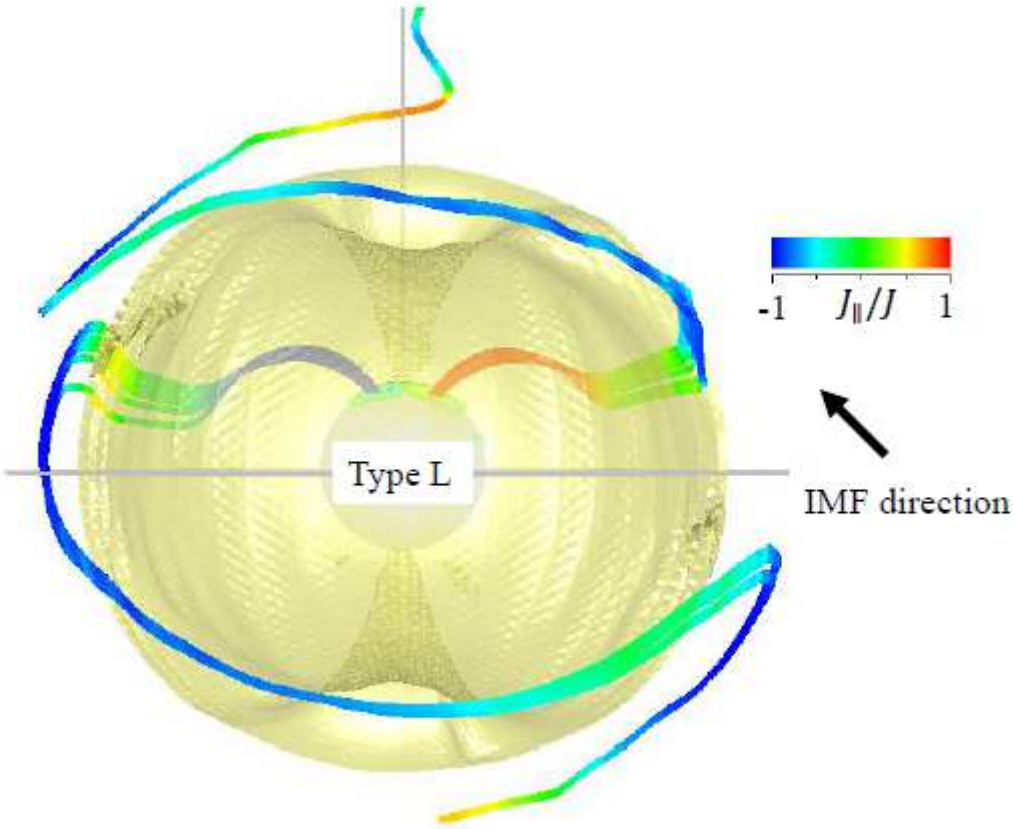

Figure 5

Overall picture of the type L current system connected to the ionosphere in the northern hemisphere, as seen from the Sun at t=5.5 min. This figure shows the type L current system from the post-noon ionosphere (the same as that in Figure 3) and that from the pre-noon ionosphere. The type L current from the pre-noon ionosphere goes to the magnetosheath in the southern hemisphere. The 3D equi-contour of the pressure seen from the Sun is shown with volume rendering. The equi-contour roughly indicates the magnetopause. The black arrow in the right indicates IMF direction.

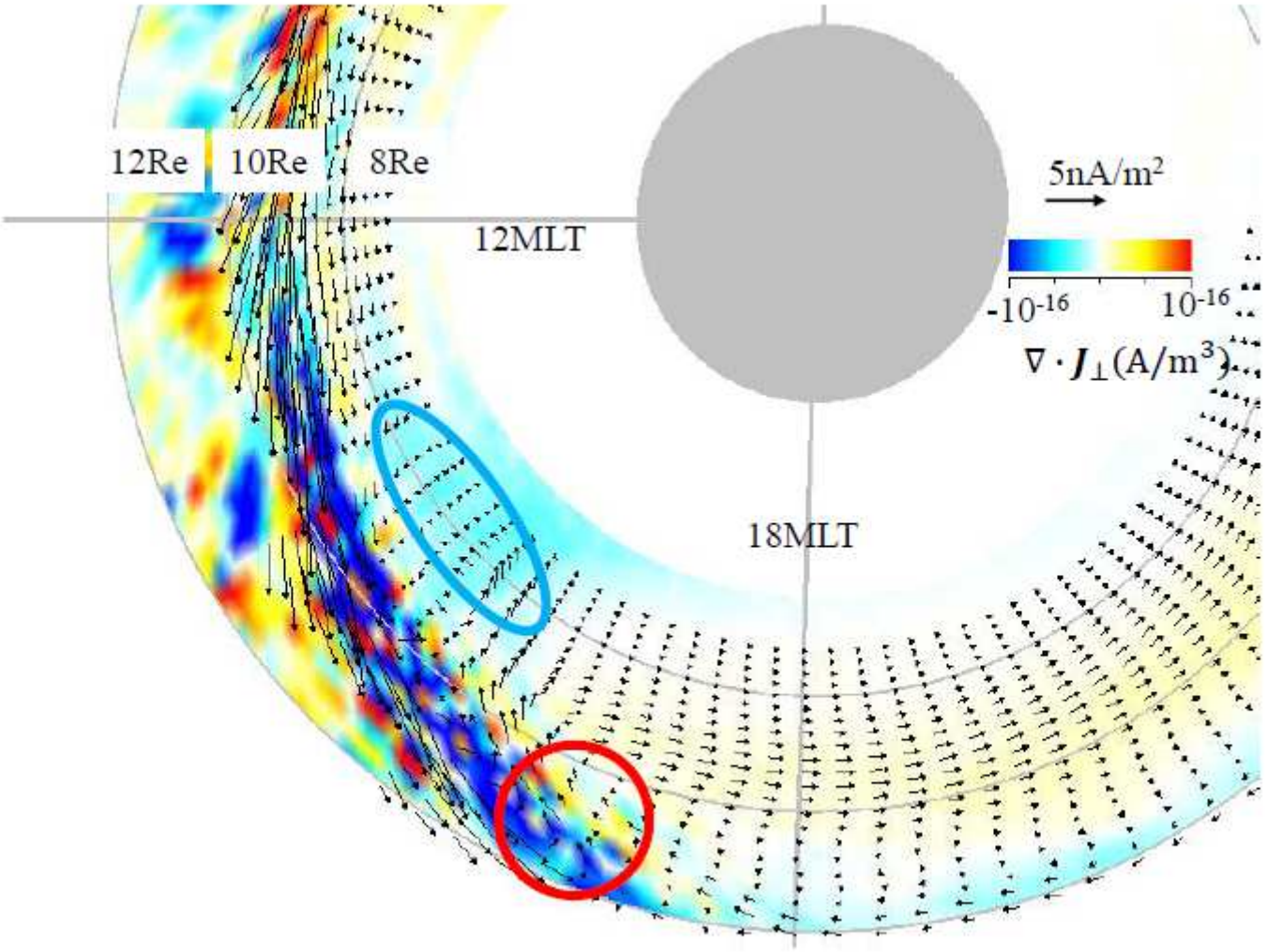

Figure 6

FPC vectors in the post-noon sector of the equatorial plane at 5.5 min. $\nabla \cdot \boldsymbol{J}_{\perp}$ values in the equatorial plane are shown with color shading. The red circle indicates the equatorial projection of the region where the cross-magnetopause current exists. The type L current flows across the magnetopause in this region. In contrast, the blue ellipse indicates the equatorial projection of the region where the type H current system converts from the FPC to the FAC. It is evident that the current exhibits negative divergence ($\nabla \cdot \boldsymbol{J}_{\perp}<0$) in the blue ellipse.

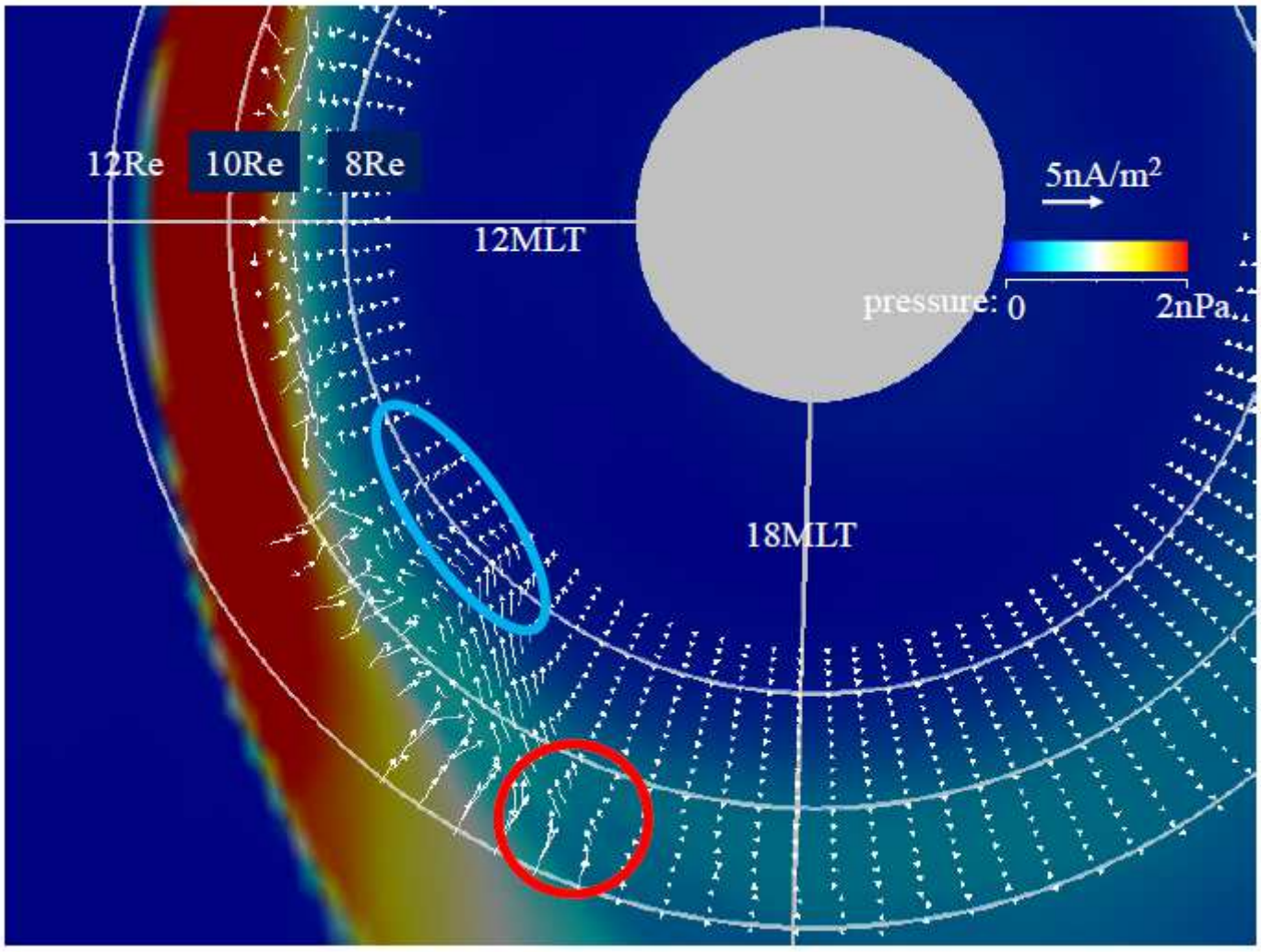

Figure 7

Vectors of the inertia current (J_i) in the post-noon sector of the equatorial plane at 5.5 min. The pressure distribution in the equatorial plane is shown with color shading. See the Figure 6 caption for descriptions of the red circle and blue ellipse.

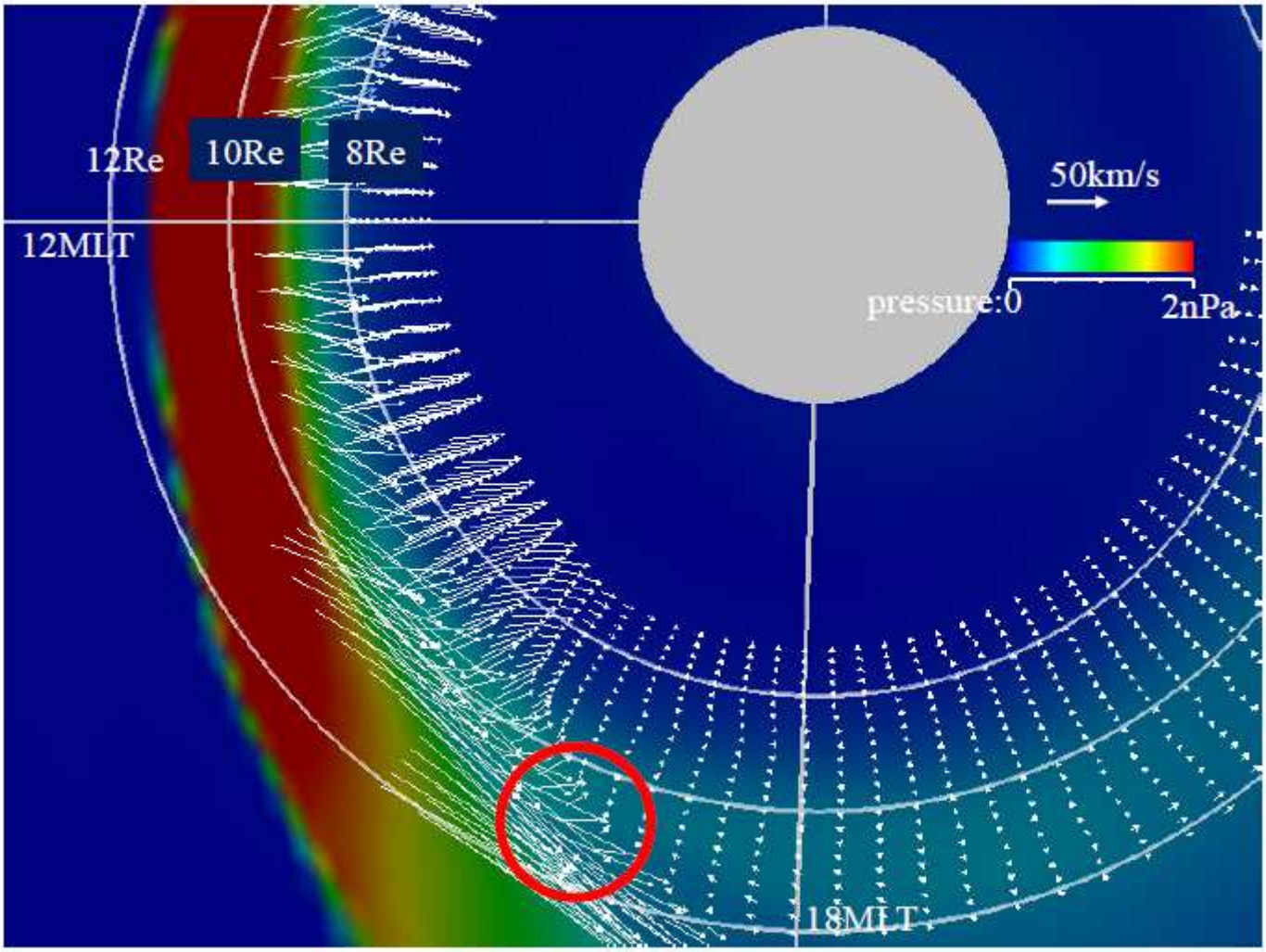

Figure 8

Vectors of the plasma flow perpendicular to the magnetic field in the post-noon sector of the equatorial plane at 5.5 min. The pressure distribution in the equatorial plane is shown with color shading. See the Figure 6 caption for the description of the red circle.

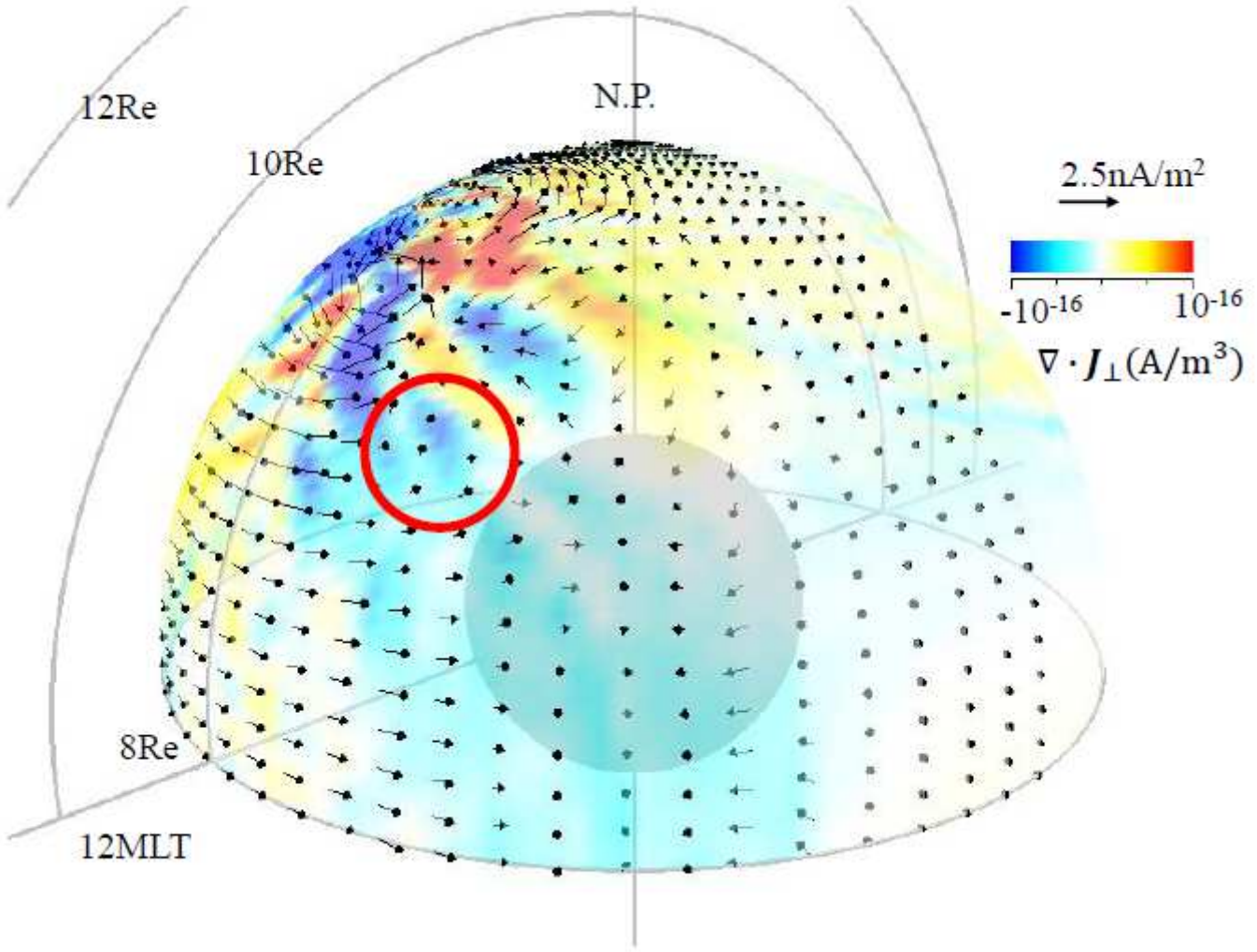

Figure 9

FPC vectors in the post-noon sector on the sphere of r=8Re in the northern hemisphere at 5.9 min. $\nabla \cdot \boldsymbol{J}_{\perp}$ on this sphere is shown with color shading. The red circle indicates the region through which the type L current system from BH passes (Figure 4).

Figure 10

See image above for figure legend.

Figure 11

See image above for figure legend.

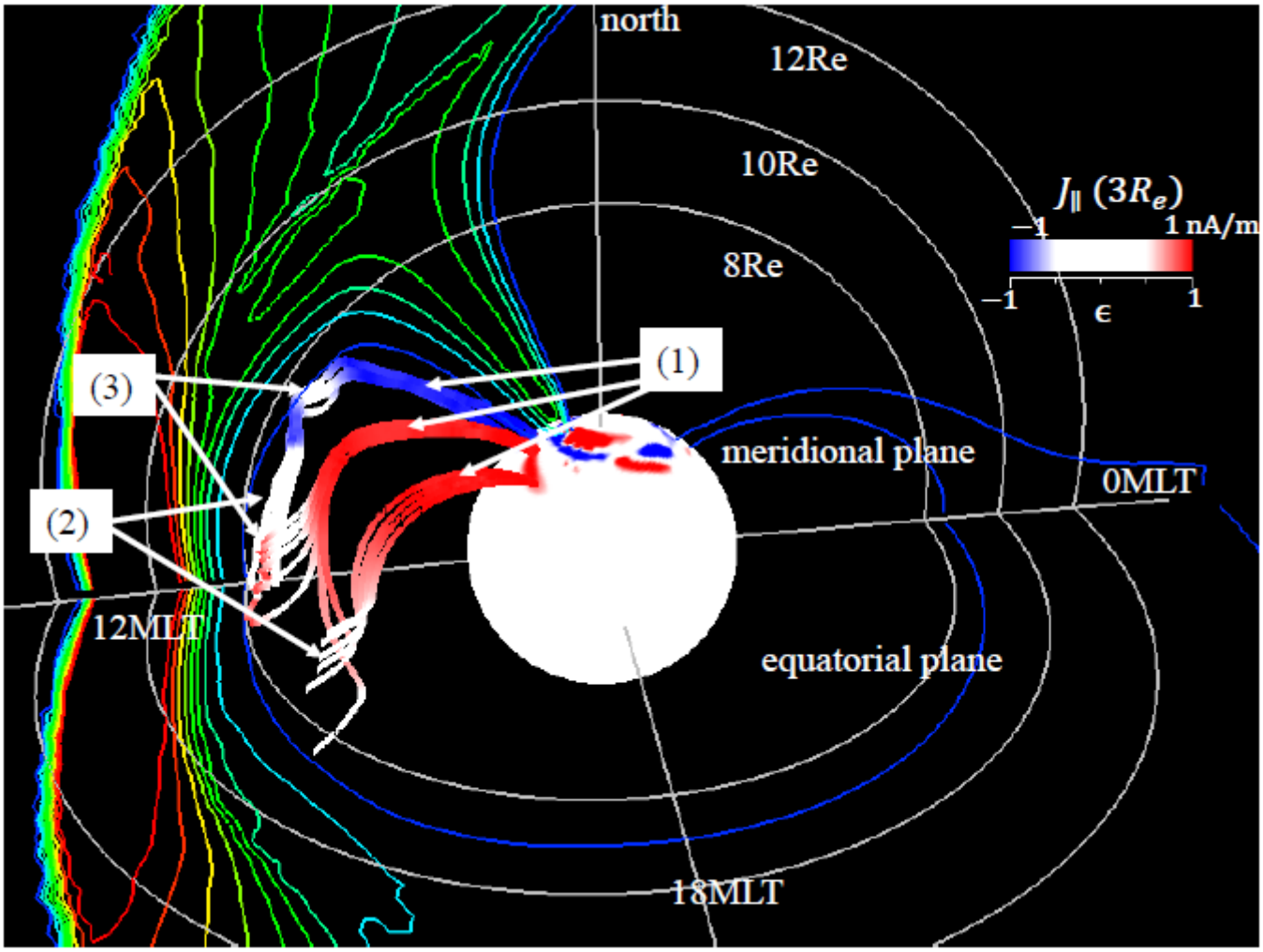

Figure 12

The type H and L current systems illustrated in the same manner used in Figure 3 at t=5.5 min according to the value of . The current lines are shown only in the area of β<0.2. The Alfven-mode current and the fast magnetosonic-mode current are dominant along the current lines denoted by (1) and (2), respectively. The mixture of the two modes appears along the current lines denoted by (3).

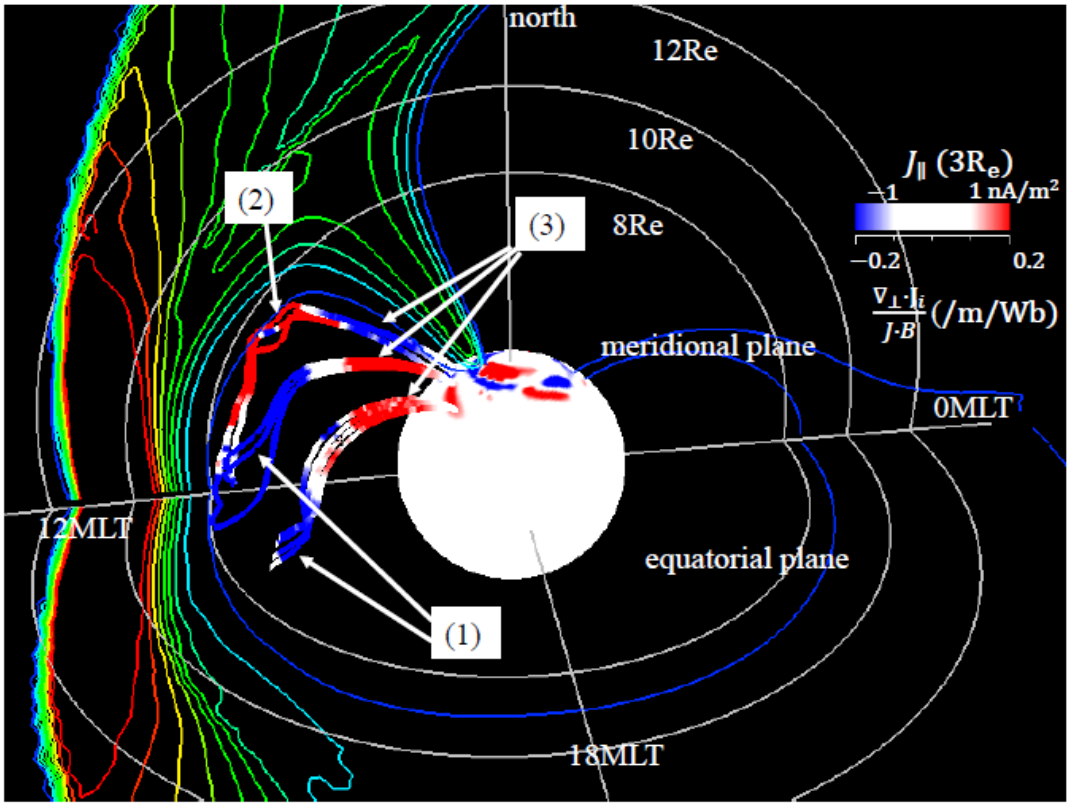

Figure 13: Type H and L current systems at t=5.5 min colored according to $\frac{\nabla_\perp \cdot \mathbf{J}_i}{JB}$ values in the same manner as in Figure 3. The current lines are shown only in the area of β<0.2. The type L current from A_H is not shown in this figure. There are three characteristic regions of the FPC-FAC conversion. The negative and positive $\frac{\nabla_\perp \cdot \mathbf{J}_i}{JB}$ in regions (1) and (2), respectively, appears in the boundary between the outer and inner magnetosphere. The region (3) is located in the lower magnetosphere.

Figure 13

See image above for figure legend.

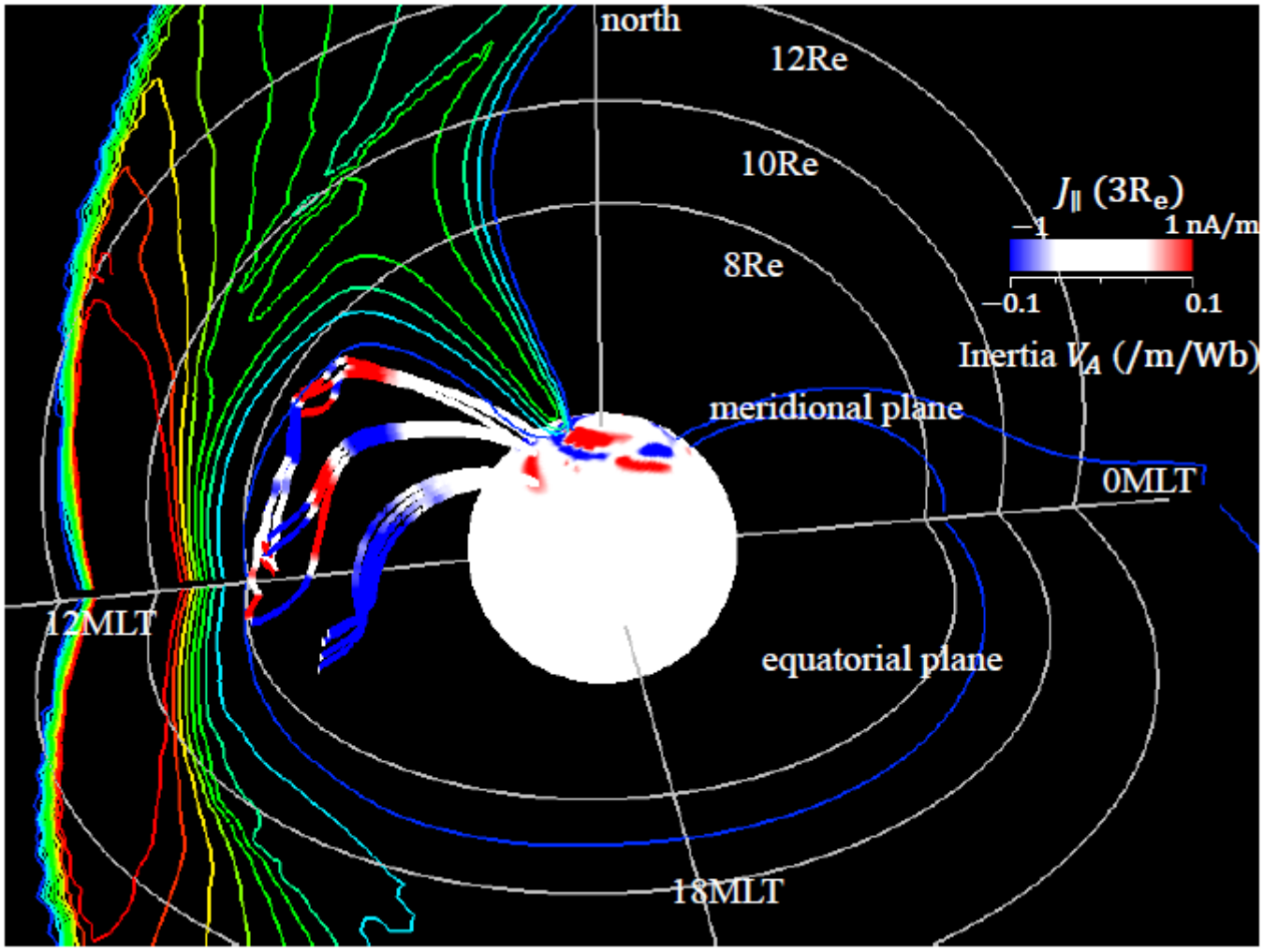

Figure 14

Type H and L current systems at t=5.5 min colored according to inertia V_A in the same manner as in Figure 3. The current lines are shown only in the area of β<0.2. The contour line colors change in increments of ±0.1. The type L current from AH is not shown in this figure.

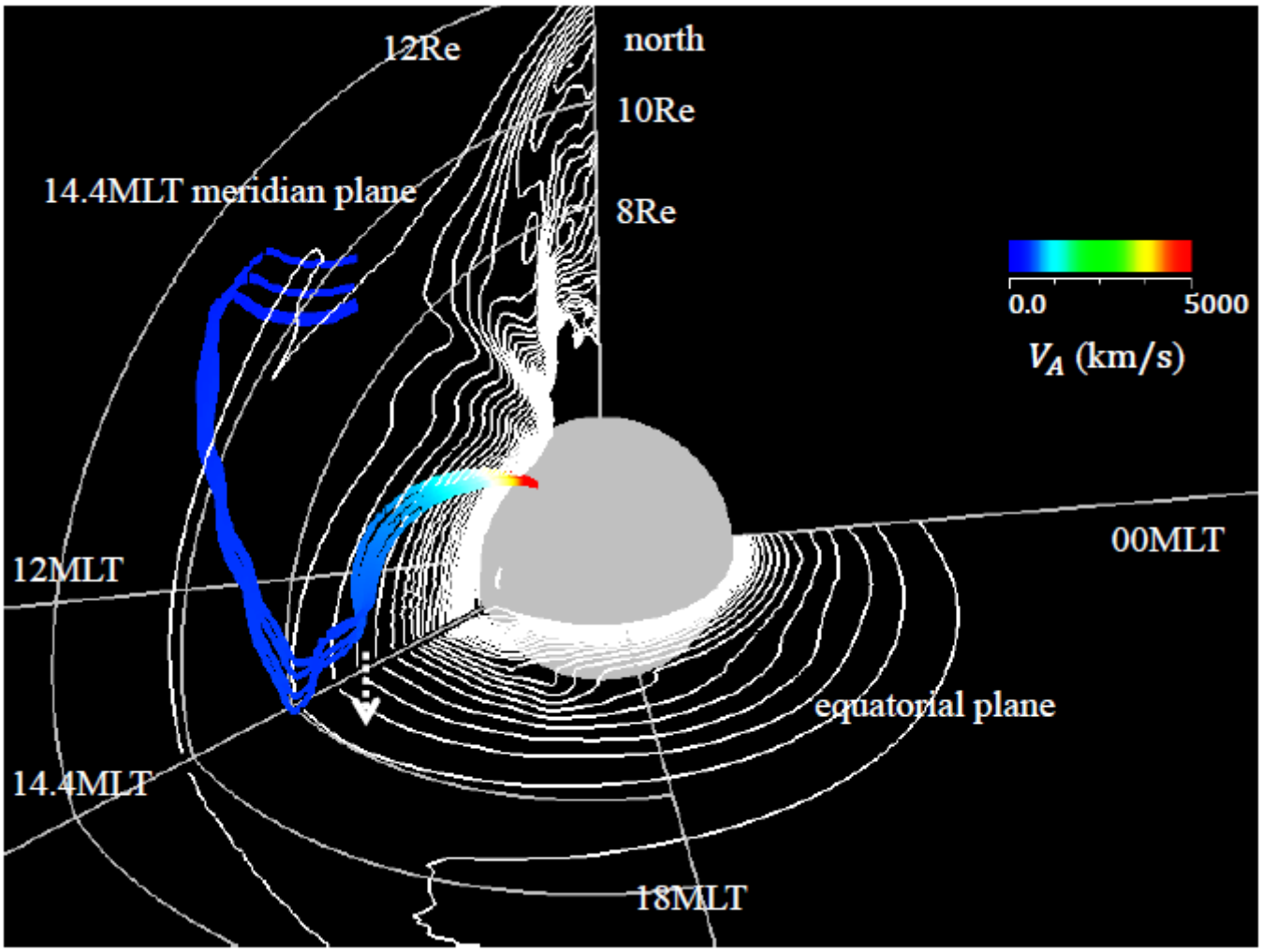

Figure 15

Distributions of V_A in the 14.4 MLT meridian plane and the equatorial plane. The type L current system that flows in the 14.4 MLT plane is also shown. The white dotted arrow indicates the L value of the field line where FPC is converted to FAC (L≈7). The color of the current lines denotes V_A .

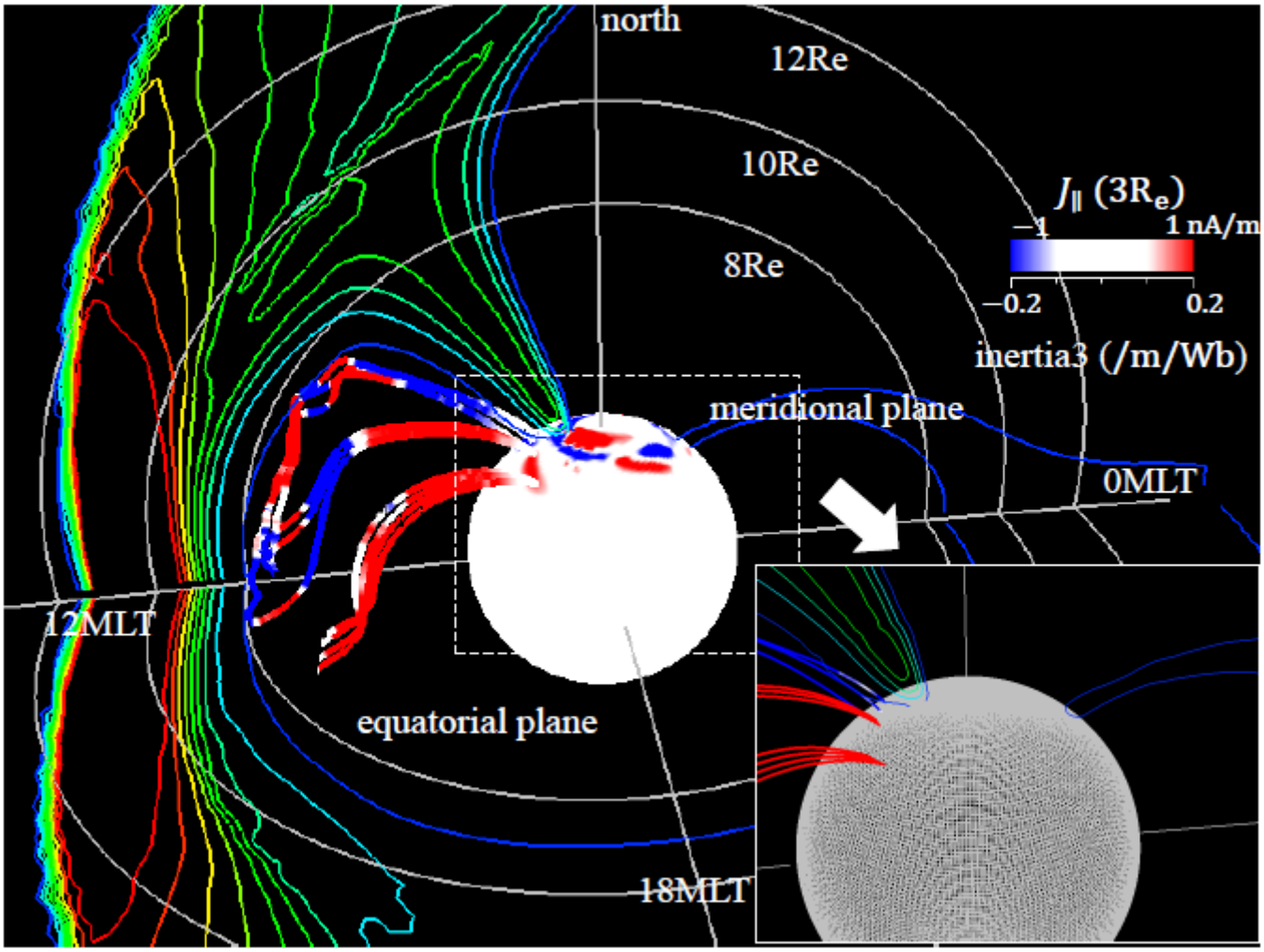

Figure 16

Type H and L current systems at t=5.5 min colored according to inertia 3 values in the same manner as in Figure 3. The current lines are shown only in the area of β<0.2. The contour line colors change in increments of ±0.2. The type L current from AH is not shown in this figure. The inset in the left-bottom corner shows an enlarged part of the footpoints of both current systems. The color scale of inertia 3 for the inset is in increments of ±0.05.

Supplementary Files

This is a list of supplementary files associated with this preprint. Click to download.

- 2021eSC2PIgraphicalabstract.png